The cerebral cavernous malformation pathway controls embryonic endocardial gene expression through regulation of MEKK3 signaling and KLF expression

Zinan Zhou[1*], David Rawnsley[1*], Lauren Goddard[1], Wei Pan[1], Xing--Jun Cao[2], Zoltan Jakus[1,9], Hui Zheng[1], Jisheng Yang[1], Simon Arthur[3], Kevin J. Whitehead[4], Dean Li[4,5], Bin Zhou[6], Benjamin A. Garcia[2], Xiangjian Zheng[1,7], and Mark L. Kahn[8]

[1]Department of Medicine and Cardiovascular Institute, University of Pennsylvania, 3400 Civic Center Boulevard, Philadelphia, PA 19104, USA.
[2]Department of Biochemistry and Biophysics, University of Pennsylvania, 3400 Civic Center Boulevard, Philadelphia, PA 19104, USA.
[3]Division of Cell Signaling and Immunology, University of Dundee, Dundee DD1 5EH, UK.
[4]Division of Cardiovascular Medicine and the Program in Molecular Medicine, University of Utah, Salt Lake City, UT 84112, USA.
[5]Division of Cardiovascular Medicine and the Program in Molecular Medicine, University of Utah, Salt Lake City, UT 84112, USA; The Key Laboratory for Human Disease Gene Study of Sichuan Province, Institute of Laboratory Medicine, Sichuan Academy of Medical Sciences & Sichuan Provincial People's Hospital, Chengdu, Sichuan 610072, China.
[6]Department of Genetics, Pediatric, and Medicine (Cardiology) and Wilf Cardiovascular Research Institute, Albert Einstein College of Medicine of Yeshiva University, 1301 Morris Park Avenue, Bronx, NY 10461, USA.
[7]Department of Medicine and Cardiovascular Institute, University of Pennsylvania, 3400 Civic Center Boulevard, Philadelphia, PA 19104, USA; Lab of Cardiovascular Signaling, Centenary Institute, Sydney NSW 2050, Australia.
[8]Department of Medicine and Cardiovascular Institute, University of Pennsylvania, 3400 Civic Center Boulevard, Philadelphia, PA 19104, USA.
[9]Present address: MTA-SE Lendulet Lymphatic Physiology Research Group of the Hungarian Academy of Sciences and the Semmelweis University, 1094 Budapest, Hungary

*These authors contributed equally

Correspondence should be addressed to: X.Z. (email: x.zheng@centenary.org.au) Telephone: 61--2--9565--6235 FAX: 61--2--9565--6101 or M.L.K. (email: markkahn@mail.med.upenn.edu) Telephone: 215--898--9007 FAX: 215--573--2094

SUMMARY

The cerebral cavernous malformation (CCM) pathway is required in endothelial cells for normal cardiovascular development and to prevent postnatal vascular malformations, but its molecular effectors are not well defined. Here we show that loss of CCM signaling in endocardial cells results in mid-gestation heart failure associated with premature degradation of cardiac jelly. CCM deficiency dramatically alters endocardial and endothelial gene expression, including increased expression of the *Klf2* and *Klf4* transcription factors and the *Adamts4* and *Adamts5* proteases that degrade cardiac jelly. These changes in gene expression result from increased activity of MEKK3, a mitogen-activated protein kinase that binds CCM2 in endothelial cells. MEKK3 is both necessary and sufficient for expression of these genes, and partial loss of MEKK3 rescues cardiac defects in CCM-deficient embryos. These findings reveal a molecular mechanism by which CCM signaling controls endothelial gene expression during cardiovascular development that may also underlie CCM formation.

INTRODUCTION

Embryonic heart growth requires the coordinated expansion and patterning of two major cell types, endothelial cells that line the lumen of the cardiac chambers and contractile myocardial cells that pump blood. These cell types support and interact with each other through secreted factors, i.e. endocardial-secreted growth factors such as neuregulin and FGFs that stimulate myocardial proliferation (Gassmann et al., 1995; Lavine et al., 2005) and myocardial-derived factors such as angiopoietin (Jeansson et al., 2011) that support endocardial growth. Loss of endocardial-myocardial signaling results in a failure of cardiac growth and embryonic lethality (Gassmann et al., 1995). Similar phenotypes arise in human patients with cardiac non-compaction (Jenni et al., 1999).

During the early, most rapid period of cardiac growth (E8.5-E14.5 in the mouse), abundant extracellular matrix known collectively as cardiac jelly separates the endocardium and myocardium (Nakamura and Manasek, 1981). Cardiac jelly consists of glycoaminoglycans such as hyaluronic acid (HA), and HA-binding proteins such as versican. Loss of either HA synthase or versican results in a thin myocardium that fails to proliferate and form normal trabeculae (Camenisch et al., 2000; Yamamura et al., 1997). As the heart matures and trabeculation is completed, cardiac jelly is lost and myocardial proliferation slows. Recent genetic studies in mice have implicated endocardial expression of secreted proteases such as ADAMTS1 and ADAMTS5 that degrade versican in the regulation of cardiac jelly and heart valve formation (Dupuis et al., 2011; Stankunas et al., 2008), but the upstream signaling pathways that control endothelial expression of such proteases and thereby regulate cardiac growth remain largely unknown.

The cerebral cavernous malformation (CCM) signaling pathway was discovered through genetic studies of human patients with familial vascular malformations (Chan et al., 2010; Riant et al., 2010). These studies have identified loss of function mutations in three genes, *KRIT1*, *CCM2* and *PDCD10* (reviewed in Riant et al., 2010) that encode intracellular adaptor proteins that associate to form a biochemical complex with the transmembrane protein Heart of Glass (HEG1) (Kleaveland et al., 2009; Zheng et al., 2010). Conditional deletion studies in mice have demonstrated that KRIT1 and CCM2 are required in endothelial cells for branchial arch artery formation at E8.5-9 (Whitehead et al., 2009; Whitehead et al., 2004; Zheng et al., 2010), and to prevent CCM formation in the central nervous system of postnatal animals (Boulday et al., 2011; Chan et al., 2011; McDonald et al., 2011). How CCM signaling regulates endothelial and vascular function remains unclear. Cell culture studies and pharmacologic studies in mice have linked CCM signaling to negative regulation of RhoA activity (Glading et al., 2007; Stockton et al., 2010; Whitehead et al., 2009; Zheng et al., 2010) and TGFb (Maddaluno et al., 2013), but definitive evidence for a causal relationship to these pathways or other downstream CCM effectors that clearly explain the pathway's function in vascular development and maintenance has been lacking.

A role for CCM signaling in the developing heart was first revealed by zebrafish embryos lacking *heg1, krit1, ccm2,* and *pdcd10* that exhibited a characteristic dilated heart phenotype (Mably et al., 2006; Mably et al., 2003; Zheng et al., 2010). In the developing mouse, *Heg* is strongly expressed in the endocardium and its loss results in patchy areas of thin myocardium and cardiac rupture in late gestation (Kleaveland et al., 2009; Zheng et al., 2012). We have also recently identified a CCM2 orthologue,

CCM2L, that is expressed selectively in the endocardium of the developing heart where it regulates cardiac growth (Zheng et al., 2012). A major impediment to defining the role of the CCM pathway in cardiac development in mice has been early lethality due to vascular defects that prevent blood circulation. In the present study we use an *Nfatc1*^{Cre} allele to delete CCM pathway genes specifically in the endocardium and bypass this vascular requirement (Wu et al., 2012). We find that loss of endocardial CCM signaling results in embryonic heart failure and reduced myocardial growth that is characterized by loss of cardiac jelly and preserved expression of endocardial growth factors. This phenotype is caused by increased expression of the *Klf2* and *Klf4* transcription factors and the *Adamts4* and *Adamts5* proteases that degrade the cardiac jelly protein versican. CCM-deficient endothelial gene expression changes are associated with increased activity of the MEKK3 signaling pathway, and CCM-deficient changes in cultured endothelial cells and embryonic mouse and fish hearts are rescued by reduced MEKK3 expression or activity. These studies define regulation of MEKK3 signaling and endothelial gene expression as a conserved mechanism by which CCM signaling functions in the developing heart, and raise the possibility that loss of this molecular regulatory mechanism may also participate in CCM formation.

RESULTS

Nfatc1^{Cre} drives recombination in the endocardium but not in the endothelium of developing BAAs or peripheral vessels

Previous studies of global and endothelial-specific loss of *Krit1* and *Ccm2* revealed embryonic lethality at E8.5-9.5 due to a lack of lumenized branchial arch arteries (BAAs) and blood circulation (Boulday et al., 2009; Whitehead et al., 2009; Whitehead et al., 2004; Zheng et al., 2010), a severe vascular phenotype that was also observed in zebrafish embryos lacking HEG-CCM signaling (Zheng et al., 2010). Cardiac defects, such as atrial enlargement, reduced trabeculation and pericardial edema, were noted in deficient mouse embryos (Boulday et al., 2009; Whitehead et al., 2004), but since these changes arose in animals with complete vascular disruption it was not clear if they were primary or secondary phenotypes.

To circumvent the early requirement for CCM signaling in the BAA endothelium and investigate the role of CCM signaling specifically in the heart, we used *Nfatc1^{Cre}* mice (Wu et al., 2012). Consistent with published studies, lineage tracing studies in *Nfatc1^{Cre}*;R26R-YFP animals revealed *Nfatc1^{Cre}* activity throughout the atrial and ventricular endocardium, but not in the endothelium of the distal aortic sac or the developing BAAs at E10.5 (Fig. S1A-F). *Nfatc1^{Cre}* activity was observed in endothelial cells of the ascending aorta and proximal pulmonary arteries at E14.5, but not in more distal great vessels at that timepoint (Fig. S1G-K) or in the endothelial cells of the peripheral vasculature in the liver or kidney at P1 (Fig. S1L-R). These studies suggested that *Nfatc1^{Cre}* could be used to test the requirement for CCM signaling specifically within the endocardium of the developing heart.

Endocardial deletion of Krit1 results in mid-gestation heart failure associated with loss of cardiac jelly.

Analysis of *Nfatc1*^{Cre};*Krit1*$^{fl/+}$ X *Krit1*$^{fl/fl}$ crosses at P0.5 revealed that *Nfatc1*^{Cre};*Krit1*$^{fl/fl}$ mice die prior to birth (Supp. Table 1). Timed matings demonstrated live *Nfatc1*^{Cre};*Krit1*$^{fl/fl}$ embryos that were grossly indistinguishable from littermate controls at E12.5 (Fig. S2), but all *Nfatc1*^{Cre};*Krit1*$^{fl/fl}$ embryos were dead by E14.5-15.5 (Fig. S2 and Table S1). Thus endocardial loss of KRIT1 results in embryonic lethality during mid-gestation.

To understand the cause of lethality, *Nfatc1*^{Cre};*Krit1*$^{fl/fl}$ and control littermates were examined at E10.5 and E12.5, timepoints prior to lethality. H-E staining of *Nfatc1*^{Cre};*Krit1*$^{fl/fl}$ hearts at E10.5 revealed thin myocardium and smaller myocardial trabeculae compared with littermate controls, despite the presence of abundant endocardial cells (Fig. 1A, B). These changes were more marked at E12.5, when control hearts had developed a thicker compact myocardium and well-developed trabeculae (Fig. 1C, D). Atrial and ventricular chamber dilatation, like that observed in ccm-deficient zebrafish embryos (e.g. Fig. 4 and (Mably et al., 2006; Mably et al., 2003)), were also observed in *Nfatc1*^{Cre};*Krit1*$^{fl/fl}$ embryos at E12.5 (e.g. Fig. 1C vs. 1D). Most striking was the reduction in space between the endocardium and myocardium that is occupied by cardiac jelly in *Nfatc1*^{Cre};*Krit1*$^{fl/fl}$ embryo hearts at E10.5 and E12.5 (Fig. 1A-D). This phenotype was particularly evident in the trabeculae, where the myocardium was wrapped tightly by endocardium in the *Nfatc1*^{Cre};*Krit1*$^{fl/fl}$ heart but clearly separated from the endocardium in control hearts at these timepoints (arrows, Fig. 1A-D). Quantitation

of the area occupied by cardiac jelly in the trabeculae of the E10.5 heart revealed an >65% decrease in *Nfatc1*^{Cre};*Krit1*$^{fl/fl}$ hearts compared with either *Krit1*$^{fl/fl}$ or *Nfatc1*^{Cre};*Krit1*$^{fl/+}$ littermate hearts (Fig. 1E).

The loss of endocardial-myocardial separation in *Nfatc1*^{Cre};*Krit1*$^{fl/fl}$ hearts suggested that endocardial loss of CCM1 results in reduced cardiac matrix/jelly. Consistent with this observation, Alcian blue staining demonstrated loss of matrix glycosaminoglycans in the *Nfatc1*^{Cre};*Krit1*$^{fl/fl}$ heart, particularly surrounding the trabeculae at E10.5 (Fig. 1F, G). Versican is the major protein component of cardiac jelly, and loss of versican results in reduced myocardial growth and failure to form myocardial trabeculae. Immunostaining revealed a severe loss of intact versican in the E10.5 *Nfatc1*^{Cre};*Krit1*$^{fl/fl}$ heart compared with controls (Fig. 1H, I). Thus endocardial loss of KRIT1 results in mid-gestation heart failure associated with reduced cardiac jelly.

Endocardial loss of Ccm2 and Pdcd10 also result in loss of cardiac jelly.

In the CCM signaling pathway KRIT1 binds CCM2 and CCM2 binds PDCD10 to form a ternary complex (Hilder et al., 2007; Zawistowski et al., 2005; Zhang et al., 2007), and deficiency of any of these three proteins results in CCM formation in human patients and in mouse models of postnatal endothelial deficiency (Boulday et al., 2009; Boulday et al., 2011; Whitehead et al., 2009; Whitehead et al., 2004). However, KRIT1 also regulates integrin affinity through its interaction with ICAP1 (Liu et al., 2013) and binds RAP1 (Serebriiskii et al., 1997). Thus the role of KRIT1 in the endocardium of the developing heart might not simply reflect the role for CCM signaling in that cell type. To test whether the cardiac abnormalities described above arise due to loss of canonical

CCM signaling in the endocardium, we deleted *Ccm2* and *Pdcd10* in the endocardium using $Nfatc1^{Cre}$. $Nfatc1^{Cre};Ccm2^{fl/fl}$ embryos exhibited embryonic lethality at the same timepoint as observed for $Nfatc1^{Cre};Krit1^{fl/fl}$ embryos (Table S1). $Nfatc1^{Cre};Ccm2^{fl/fl}$ embryos also exhibited similar reductions in cardiac jelly, myocardial growth, Alcian blue staining and cardiac versican at both E10.5 (Fig. 2A-F) and E12.5 (Fig. 2G-L). $Nfatc1^{Cre};Pdcd10^{fl/fl}$ embryos exhibited embryonic lethality that was later than that as observed for $Nfatc1^{Cre};Krit1^{fl/fl}$ and $Nfatc1^{Cre};Ccm2^{fl/fl}$ embryos (Table S1). $Nfatc1^{Cre};Pdcd10^{fl/fl}$ embryos did not appear abnormal at E10.5, but reduced cardiac jelly, myocardial growth, Alcian blue staining and versican were observed at E12.5 (Fig. 2M-R), consistent with a milder presentation of the same phenotype. These findings suggest that all three primary components of the CCM signaling pathway function in the mid-gestation endocardium to maintain cardiac jelly and support cardiac growth.

Endocardial loss of KRIT1 is associated with changes in the expression of KLF2/4 transcription factors and ADAMTS4/5 proteases.

The thin myocardium and reduced cardiac jelly observed in $Nfatc1^{Cre};Krit1^{fl/fl}$ hearts could result from reduced endocardial expression of myocardial growth factors and components of the cardiac jelly such as hyluronic acid. Alternatively, endocardial CCM signaling might be required to prevent the expression of proteases such as those in the ADAMTS family that cleave versican and degrade cardiac jelly at later timepoints during cardiac development (Stankunas et al., 2008; Dupuis et al., 2011). To address these possible mechanisms we characterized gene expression in whole E10.5 $Nfatc1^{Cre};Krit1^{fl/fl}$ and littermate control hearts using microarray and qPCR analysis. Microarray and qPCR

analysis revealed elevated levels of *Adamts4* and *Adamts5*, versican-degrading proteases, in addition to *Klf2* and *Klf4* and a number of known KLF2/4 target genes, including *Nos3, Aqp1, Jam2, Thbd,* and *Palmd* (Dekker et al., 2006; Parmar et al., 2006) (Fig. 3A, B & D). Reduced levels of *Dll4* and *Tmem100*, genes previously associated with myocardial growth and trabeculation (Grego-Bessa et al., 2007; Somekawa et al., 2012), were also detected (Fig. 3A, C). Expression of the myocardial growth factors FGF9, FGF12 and FGF16 (Lavine et al., 2005) was unaltered, while that of neuregulin was elevated in E10.5 $Nfatc1^{Cre}$;$Krit1^{fl/fl}$ hearts (Fig. 3C), indicating that reduced myocardial growth did not result from reduced endocardial expression of growth factors. The expression of *Versican* and *HA synthase* were also unchanged, despite the dramatic loss of versican protein detected in $Nfatc1^{Cre}$;$Krit1^{fl/fl}$ hearts (Fig. 3D). In situ hybridization confirmed the increase in *Klf2* mRNA in the E10.5 $Nfatc1^{Cre}$;$Krit1^{fl/fl}$ heart (Fig. 3E). KLF4 protein was not detected in the endocardium of the heart chamber in control animals at E10.5, but was present in the nuclei of almost all the endocardial cells in the E10.5 $Nfatc1^{Cre}$;$Krit1^{fl/fl}$ heart (Fig. 3F). Increased levels of KLF2 protein were also detected by western blot analysis of the E10.5 $Nfatc1^{Cre}$;$Krit1^{fl/fl}$ heart (Fig. 3G). Significantly, similar changes in *Klf* and *Adamts* gene expression were observed in the E11.5 $Nfatc1^{Cre}$;$Pdcd10^{fl/fl}$ heart (Fig. S2), consistent with a requirement for canonical CCM signaling in the regulation of these genes.

The gene expression studies described above suggested that excess ADAMTS4/5 activity might be the cause of reduced versican and cardiac jelly in $Nfatc1^{Cre}$;$Krit1^{fl/fl}$ hearts. To detect ADAMTS-mediated breakdown of versican we stained $Nfatc1^{Cre}$;$Krit1^{fl/fl}$ and control E10.5 hearts with antibodies that specifically recognize a

versican epitope that is exposed following cleavage by ADAMTS proteases ("DPEAAE" antibody) (Sandy et al., 2001). Despite the nearly complete loss of intact versican (Fig. 1H, I), increased levels of ADAMTS-cleaved versican were detected in the E10.5 *Nfatc1*^{Cre};*Krit1*$^{fl/fl}$ heart by immunostaining with DPEAAE antibody (Fig. 3H). Biochemical analysis of whole E10.5 *Nfatc1*^{Cre};*Krit1*$^{fl/fl}$ hearts confirmed a marked increase in the levels of cleaved versican and ADAMTS5 protease (Fig. 3I). These findings tie the loss of cardiac jelly associated with endocardial loss of CCM signaling to changes in endocardial gene expression.

Loss of klf2 or adamts5 rescues loss of CCM signaling in zebrafish embryos.

Endocardial-specific loss of CCM signaling in the mouse results in a thin, dilated heart that lacks cardiac jelly/matrix (Figs. 1 & 2). This phenotype resembles the dilated heart in zebrafish embryos lacking this pathway (Mably et al., 2006; Mably et al., 2003), suggestive of a conserved role for CCM signaling in vertebrate cardiac development. To determine if loss of CCM signaling results in loss of cardiac jelly/matrix in developing fish as well as mice we analyzed sections of 72 hpf *ccm2* mutant and control littermate hearts using H-E and Alcian blue staining. Control hearts exhibited a multicellular layer of myocardium, with detectable Alcian blue-stained cardiac jelly between the endocardial and myocardial cell layers (Fig. 4A, B, C). In contrast, *ccm2* mutant hearts exhibited a thin, single-cell layer of myocardium, and no Alcian blue staining was detected in sections that sampled the entire heart (Fig. 4D, E, F, N=4 embryos studied for each genotype). Thus CCM signaling deficiency results in the loss of cardiac jelly in both fish

and mouse embryos, consistent with a conserved role for this pathway during heart development.

Molecular analysis of E10.5 *Nfatc1*^{Cre};*Krit1*$^{fl/fl}$ and E10.5 *Nfatc1*^{Cre};*Pdcd10*$^{fl/fl}$ mouse hearts revealed significant up-regulation of *Klf2/4* and *Adamts4/5* gene expression, suggesting that these genes might play causal roles in the cardiac phenotype. To functionally test a conserved role for regulation of KLF2 and ADAMTS5 by CCM signaling we next studied 72 hpf zebrafish embryos following injection of morpholinos to block expression of *krit1*, with or without co-injection of morpholinos to block *klf2*a and *klf2*b (the two zebrafish *Klf2* orthologues) or *adamts5* (the sole zebrafish *Adamts5* orthologue). *krit1* morpholinos resulted in a dilated heart in approximately 80% of embryos at 72 hpf (Fig. 4G, J). When combined with low dose *klf2*a/b morpholinos (1.5 ng each) that resulted in a reduction of approximately 50% in *klf2* dosage (Fig. S3), we observed highly efficient rescue of the big heart phenotype (approximately 90% rescue efficiency, $P<0.001$) (Fig. 4H, J). Co-injection of morpholinos targeting the exon 2 splice acceptor and donor sites of *adamts5* (5+1 ng, a combination chosen to minimize morpholino dose and toxicity, Supp. Fig. 4C, D) also resulted in a significant rescue of the big heart phenotype (approximately 50% rescue efficiency, $P<0.001$) (Fig. 4I, J). To ensure that rescue was not merely due to interference with *krit1* morpholinos, *klf2* or *adamts5* morpholinos were injected into embryos generated by *ccm2*$^{+/-}$ intercrosses. As expected, a big heart phenotype was observed in approximately 25% of control offspring at 72 hpf (Fig. 4K). However, this cardiac phenotype was observed in only 7% and 16% of offspring injected with *klf2*a/b or *adamts5* morpholinos respectively (indicative of a 70% and 35% rescue efficiency for *klf2* and *adamts5* respectively; $P<0.01$ and $P<0.05$)

(Fig. 4K). The lower efficiency of mutant rescue compared with morphant rescue most likely reflects the greater loss of CCM signaling in *ccm2*$^{-/-}$ mutants compared with *krit1* morphants. These studies suggest that a critical and conserved role of CCM signaling in the developing heart is to negatively regulate the expression of *Klf2* and *Adamts5*.

MEKK3 regulates KLF and ADAMTS gene expression in cultured endothelial cells and in embryonic endocardium.

The findings described above revealed that CCM signaling negatively regulates *Klf2* and *Adamts5* gene expression, but studies of signaling by the CCM adaptor proteins have not defined a transcriptional mechanism of action. How are these pathways linked? MEKK3 was identified as a CCM2 binding partner a decade ago (Uhlik et al., 2003), and MEKK3 signaling is known to regulate gene expression through downstream effectors such as ERK5 and MEF2C (Chao et al., 1999; Nakamura and Johnson, 2003), as well as p38 and JNK (Deacon and Blank, 1999; Nebreda and Porras, 2000). We therefore next explored the possibility that CCM signaling might alter expression of KLF2 and ADAMTS5 through effects on the MEKK3 pathway. Since available anti-CCM2 antibodies are unable to detect the protein in cultured endothelial cells, to determine if MEKK3 interacts with CCM proteins in endothelial cells we used tetracycline-regulable lentiviral vectors to express an BirA-MEKK3 fusion protein in hCMEC/D3 endothelial cells (Weksler et al., 2005) (Fig. S4). Using this approach MEKK3-interacting proteins were biotinylated in live endothelial cells (Roux et al., 2012). Biotinylated proteins were captured by streptavidin beads and subjected to mass spectrometry analysis. When BirA-MEKK3 was expressed at endogenous levels (4 ng/ml doxycycline, Fig. S4A), no

specific MEKK3-interacting proteins were identified (not shown), perhaps due to kinase inactivity. At slightly higher expression levels (8 ng/ml doxycycline) peptides from only 4 interacting proteins were identified (Fig. S4). The most abundant of these was CCM2 (Fig. S4E). KRIT1 was also detected at a lower level equivalent to that of TRAF7, an MEKK3-interacting protein previously identified using tandem affinity purification (Bouwmeester et al., 2004). A similar result was obtained when BirA-MEKK3 was expressed in primary HUVECs (Fig. S4F). These studies indicate that MEKK3 interacts with the CCM protein complex in live endothelial cells.

To determine if MEKK3 regulates endothelial gene expression in a manner that might explain the changes observed following loss of CCM signaling we next tested whether MEKK3 is sufficient and/or required for *KLF* and *ADAMTS* gene expression in cultured endothelial cells. Over-expression of MEKK3 using the doxycycline regulable system described above resulted in dose-dependent increases in the levels of *KLF2* and *KLF4* expression in hCMEC/D3 endothelial cells (Fig. 5A). To determine whether MEKK3 regulates *KLF* gene expression in response to more physiologic stimuli we tested the role of MEKK3 in endothelial responses to fluid flow. Flow and fluid shear forces are established regulators of *KLF2* and *KLF4* expression in endothelial cells ex vivo (Huddleson et al., 2004; Parmar et al., 2006; Sohn et al., 2005; Villarreal et al., 2010) and in humans (Dekker et al., 2006), mice (Dekker et al., 2006; Lee et al., 2006), chick (Groenendijk et al., 2005) and fish (Vermot et al., 2009) in vivo. Up-regulation of *KLF2* in response to flow has been shown to be mediated by MEK5-ERK5 signaling(Li et al., 2008; Parmar et al., 2006), one of the pathways directly regulated by MEKK3(Chao et al., 1999; Nakamura and Johnson, 2003). Consistent with prior studies

(Parmar et al., 2006; Sohn et al., 2005), human umbilical vein endothelial cells (HUVECs) exposed to laminar shear for 16 hours exhibited increased *KLF2, KLF4* and *ADAMTS4* expression (Fig. 5B). Transfection with siRNAs directed against *MEKK3* that resulted in a 40% knockdown in *MEKK3* expression blocked the rise in expression of *KLF2, KLF4* and *ADAMTS4* induced by flow (Fig. 5B). These studies reveal that *KLF* and *ADAMTS* expression are regulated by MEKK3 in cultured endothelial cells.

To determine whether MEKK3 also regulates these genes in the E10.5 heart we next generated $Nfatc1^{Cre}$;$Map3k3^{fl/-}$ animals. $Nfatc1^{Cre}$;$Map3k3^{fl/-}$ animals did not survive to birth, and timed matings revealed embryonic lethality prior to E12.5 (Table S1). Analysis of $Nfatc1^{Cre}$;$Map3k3^{fl/-}$ embryonic heart sections revealed a thin myocardial cell layer with preserved cardiac jelly and normal endocardial-myocardial separation at E10.5 (Fig. S5A). In contrast to endocardial loss of CCM signaling, versican levels were preserved in the E10.5 $Nfatc1^{Cre}$;$Map3k3^{fl/-}$ heart (Fig. S5B). Gene expression analysis of E10.5 $Nfatc1^{Cre}$;$Map3k3^{fl/-}$ and control littermate hearts revealed severe (>90%) reductions in the expression of *Klf2* and the known KLF2 target genes *Nos3, Aqp1, Jam2, Thbd,* and *Palmd*, as well as *Klf4, Adamts4* and *Adamts5* (Fig. 5C, D). FGF gene expression was unchanged but the expression of *Nrg1* was severely reduced (Fig. 5D). Thus loss of MEKK3 confers gene expression changes that are precisely reciprocal to those conferred by loss of KRIT1 or PDCD10. To determine whether MEKK3 regulates *Klf* and *Adamts* gene expression through the ERK5 MAPK pathway we cultured wild-type E10.5 explanted hearts in the presence of BIX02189, a highly specific inhibitor of MEK5, the MAPK2K that is activated by MEKK3 and in turn activates ERK5 (Tatake et al., 2008). Treatment with BIX02189 resulted in reduced levels of *Klf2, Klf4* and

Adamts5 expression (Fig. 5E). These findings demonstrate that MEKK3 regulates *KLF* and *ADAMTS* gene expression in endothelial cells ex vivo and in endocardial cells in vivo through the MEK5-ERK5 MAPK pathway.

Loss of MEKK3 rescues loss of CCM signaling in cultured endothelial cells and zebrafish embryo hearts.

The reciprocal changes in gene expression observed with endocardial loss of CCM and MEKK3 signaling, the physical interaction between the CCM complex and MEKK3, and the preservation of *Mekk3* gene expression in $Nfatc1^{Cre}$;$Krit1^{fl/fl}$ hearts (Fig. S6A) suggested that CCM signaling might regulate endocardial gene expression by inhibiting MEKK3 function. To test the effect of loss of CCM signaling on MEKK3 function we used siRNA to knockdown *CCM2* in HUVECs and examined downstream MEKK3 signaling through ERK5. HUVECs treated with *CCM2* siRNA, but not with scrambled siRNA, exhibited increased phospho-ERK5 with no change in total ERK5 or GAPDH protein (Fig. 6A), consistent with an increase in MEKK3 pathway activity. As observed with endocardial deletion in the E10.5 mouse heart, loss of *CCM2* in HUVEC conferred increased expression of *KLF2, KLF4* and *ADAMTS4* (Fig. 6B-D). These increases were reversed by simultaneous knockdown of *MEKK3*, consistent with CCM regulation of gene expression through MEKK3.

To test whether increased MEKK3 signaling is causal for CCM-deficient phentoypes in vivo we first used morpholinos to reduce the levels of *mekk3* in *krit1* morphant and *ccm2* mutant zebrafish embryos. *krit1* morpholinos resulted in a dilated heart in approximately 65% of embryos at 72 hpf in these studies (Fig. 6E, F, H). When

combined with low dose morpholinos (3 ng) that resulted in a reduction of approximately 40% in *mekk3* dosage (Fig. S7) but had no independent effect on cardiac development, we observed efficient (approx 75%) rescue of the *krit1* morphant cardiac phenotype ($P<0.001$) (Fig. 6G, H). To ensure that rescue was not due to interference with *krit1* morpholinos, *mekk3* morpholinos were injected into embryos generated by $ccm2^{+/-}$ intercrosses. A big heart phenotype was observed in approximately 18% of control morpholino injected offspring at 72 hpf, and injection of low dose *mekk3* morpholinos reduced this to approximately 6%, consistent with a 66% rescue efficiency ($P<0.001$, Fig. 6I). Thus loss of *mekk3* rescues the dilated heart phenotype conferred by loss of either *krit1* or *ccm2* in zebrafish embryos, suggesting that gain of MEKK3 signaling may underlie the role of CCM signaling during cardiac development.

Mekk3 haplo-insufficiency rescues the loss of cardiac jelly and changes in gene expression conferred by endocardial Krit1 deletion.

Rescue of the big heart phenotype conferred by loss of CCM signaling with loss of *mekk3* expression in the zebrafish requires careful dosing of *mekk3* morpholinos to avoid an independent mekk3-deficient cardiac defect, and the ability to measure rescue using specific molecular and cellular endpoints is limited in the zebrafish embryo heart. To address these issues and rigorously test the causal role of the MEKK3 pathway as a downstream CCM effector in mammals we next tested the ability of loss of one *Mekk3* allele to rescue the specific changes in cardiac jelly and cardiac gene expression in the E10.5 $Nfatc1^{Cre}$;$Krit1^{fl/fl}$ mouse heart. Despite the expected loss in MEKK3 protein in $Map3k3^{+/-}$ hearts (Fig. S6C), $Map3k3^{+/-}$ animals and $Nfatc1^{Cre}$;$Map3k3^{fl/+}$ animals

develop normally, exhibit no changes in cardiac jelly, and have patterns of cardiac gene expression at E10.5 that are indistinguishable from *Map3k3*$^{fl/fl}$ littermates ((Yang et al., 2000) and data not shown). Thus loss of a single *Mekk3* allele is well-tolerated and does not affect cardiac development. At E10.5 *Nfatc1*^{Cre};*Krit1*$^{fl/fl}$;*Map3k3*$^{fl/+}$ hearts exhibited significantly more cardiac jelly, alcian blue staining and intact versican than was seen in *Nfatc1*^{Cre};*Krit1*$^{fl/fl}$;*Map3k3*$^{+/+}$ littermates (Fig. 7A-I). Quantitation of the area occupied by cardiac jelly in the trabeculae of E10.5 littermate hearts revealed a >65% decrease in *Nfatc1*^{Cre};*Krit1*$^{fl/fl}$ hearts compared with control littermates, but only a 25% decrease in *Nfatc1*^{Cre};*Krit1*$^{fl/fl}$;*Map3k3*$^{fl/+}$ hearts ($P<0.001$, Fig. 7J). Consistent with the rescue of cardiac jelly, biochemical analysis of ADAMTS-proteolyzed versican using anti-DPEAAE antibodies revealed increased versican breakdown in the *Nfatc1*^{Cre};*Krit1*$^{fl/fl}$ heart that was restored to normal levels in the *Nfatc1*^{Cre};*Krit1*$^{fl/fl}$;*Map3k3*$^{fl/+}$ heart (Fig. 7K). qPCR analysis of cardiac gene expression revealed significantly reduced levels of *Klf2, Klf4*, KLF2/4 target genes, *Adamts4* and *Adamts5,* and *Nrg1,* and increased levels of *Dll4* and *Tmem100*, in the *Nfatc1*^{Cre};*Krit1*$^{fl/fl}$;*Map3k3*$^{fl/+}$ heart compared with the *Nfatc1*^{Cre};*Krit1*$^{fl/fl}$;*Map3k3*$^{+/+}$ heart (Fig. 7L-N). The levels of *Klf2, Klf4* and *Adamts5* gene expression were not restored to normal in the *Nfatc1*^{Cre};*Krit1*$^{fl/fl}$;*Map3k3*$^{fl/+}$ heart, consistent with the significant but incomplete histologic rescue. Thus virtually all of the hallmark histologic, biochemical, and genetic changes observed with endocardial loss of KRIT1 are rescued by endocardial loss of MEKK3, indicating that gain of MEKK3 signaling plays a central, causal role in the endothelial phenotype conferred by loss of CCM signaling in the developing heart.

DISCUSSION

Genetic studies in humans, mice and fish have revealed that CCM signaling is required in endothelial cells for normal cardiovascular development and to prevent vascular malformations after birth, but the molecular basis for these phenotypes has remained elusive. We have used studies of cultured endothelial cells, endocardial-specific deletion in the developing mouse, and genetic rescue of the CCM-deficient heart phenotype in both mice and zebrafish to reveal a molecular mechanism by which the CCM pathway regulates endothelial gene expression. Our studies demonstrate that CCM signaling in the endocardium plays a critical and conserved role in cardiac development through regulation of the MEKK3 MAPK signaling pathway and downstream ADAMTS and KLF gene expression.

A role for CCM signaling in cardiac development was revealed by the dilated heart phenotype observed in zebrafish embryos lacking this pathway (Mably et al., 2006; Mably et al., 2003; Zheng et al., 2010), but the molecular and cellular basis for this phenotype has been unclear. The studies reported here demonstrate that CCM signaling controls degradation of cardiac jelly by negatively regulating endocardial expression of ADAMTS4/5 and KLF2/4. A causal role for excess ADAMTS4/5 is demonstrated by a dramatic increase in versican cleavage associated with loss of cardiac jelly in the *Nfatc1*^{Cre};*Krit1*$^{fl/fl}$ mouse heart and by rescue of the zebrafish dilated heart with morpholinos that reduced *adamts5* levels. Expression of both *Adamts* and *Klf* genes is severely reduced following endothelial loss of MEKK3 in vitro and in vivo, increased MEKK3 drives expression of both genes in cultured endothelial cells, rescue of *krit1* morphant and *ccm2* mutant zebrafish hearts was highly efficient with loss of *mekk3, klf2*

or *adamts5*, and both the histologic and molecular phenotypes conferred by loss of endocardial CCM signaling are rescued by partial loss of MEKK3. Thus a straightforward pathway is one in which changes in MEKK3 signaling alter expression of KLF2/4 that in turn controls expression of ADAMTS4/5 (Fig. 7O). However, *Adamts5* has not been identified as a KLF2 target gene in cultured endothelial cells (Dekker et al., 2002; Parmar et al., 2005), and we do not detect *Adamts5* expression in HUVEC. Thus *Adamts4/5* may be regulated by MEKK3 in a KLF-independent manner, or by KLF2/4 in embryonic endocardium but not in cultured endothelial cells. It is also likely that MEKK3-regulated and KLF-regulated genes other than *Adamts4/5* contribute to the cardiac phenotype associated with CCM deficiency. Two such candidates identified by our gene expression studies are *Dll4*, a Notch ligand expressed by the endocardium that supports trabeculation and myocardial proliferation (Grego-Bessa et al., 2007), and *Tmem100*, an ALK1 target gene that is also specifically expressed in the endocardium and required for cardiac growth (Somekawa et al., 2012). In this regard it is intriguing that KLF4 has recently been shown to repress Dll4 expression in endothelial cells (Hale et al., 2014).

A key finding to emerge from our studies is the identification of a molecular mechanism by which CCM signaling regulates endothelial gene expression. Previous studies of the CCM pathway have not revealed a molecular path to transcriptional regulation, although changes in RhoA activity (Glading et al., 2007; Stockton et al., 2010; Whitehead et al., 2009; Zheng et al., 2010) and TGFb signaling (Maddaluno et al., 2013) have been reported. The findings that CCM2 interacts with MEKK3 in endothelial cells and that endocardial loss of CCM signaling and MEKK3 confer precisely reciprocal

changes in gene expression suggested that the CCM pathway may control gene expression by regulating MEKK3 signaling (Fig. 7O). Rescue of CCM-deficient phenotypes in cultured endothelial cells and fish and mouse embryos demonstrates a clear causal role for increased MEKK3 function. Previous studies have linked MEKK3 to three downstream MAPK pathways by which it might regulate gene expression: JNK (Deacon and Blank, 1999), p38 (Deacon and Blank, 1999; Uhlik et al., 2003) and ERK5 (Chao et al., 1999; Nakamura and Johnson, 2003). However, our endothelial studies demonstrate MEKK3 regulation of KLF2/4 and ADAMTS4 expression in response to fluid flow, known to be downstream of MEK5 and ERK5 (Li et al., 2008; Parmar et al., 2006; Sohn et al., 2005), and ex vivo embryonic heart culture studies using a highly specific MEK5 inhibitor identify the MEK5-ERK5 pathway as a key mechanism of gene regulation by CCM signaling (Fig. 5). Thus our studies support a mechanism in which CCM signaling specifically regulates the MEK5-ERK5 pathway downstream of MEKK3 in endothelial cells.

A final question raised by our studies is whether regulation of the MEKK3 pathway by CCM signaling observed in the developing heart also plays an important role in the formation of CCMs in humans and mice. Loss of CCM signaling in the postnatal endothelium results in large vascular malformations (CCMs) in the central nervous of humans and mice (Akers et al., 2009; Boulday et al., 2011; Chan et al., 2011; McDonald et al., 2011). CCMs are an important cause of stroke for which there is presently no medical treatment (Li and Whitehead, 2010). Drugs that inhibit RhoA and TGFb signaling have been reported to reduce lesion frequency in mouse models of CCM (Maddaluno et al., 2013; McDonald et al., 2012), but the responses have been incomplete

and a clear molecular and/or cellular basis for CCM formation is still lacking. Significantly, up-regulation of KLF4 expression was recently identified as a prominent molecular phenotype of the endothelial cells that form CCMs (Maddaluno et al., 2013), a finding that mirrors the increase in KLF4 observed in the developing endocardium and in cultured endothelial cells lacking CCM signaling. It is therefore possible that CCM-deficient endothelial cells in the central nervous system exhibit increased MEKK3 activity like that we have observed in CCM-deficient endocardial cells, and that changes in gene expression resulting from increased MEKK3 activity also underlie CCM disease pathogenesis. Future studies that test rescue of CCM formation in mice using either genetic or pharmacologic loss of MEKK3 pathway activity should be able to test this clinically important hypothesis.

EXPERIMENTAL PROCEDURES

Mice

Nfatc1^{Cre} (Wu et al., 2012), *Ccm2*$^{fl/fl}$ (Zheng et al., 2012), *Pdcd10*$^{fl/fl}$ (Chan et al, 2010) and *Krit1*$^{fl/fl}$(Mleynek et al., 2014) animals have been previously described. The ROSA26-YFP reporter line was obtained from Jackson Laboratories (#006148). *Map3k3*$^{fl/fl}$ animals were generated as shown in Fig. S6. The University of Pennsylvania Institutional Animal Care and Use Committee approved all animal protocols.

Histology

Embryos and tissues were fixed in 10% formaldehyde overnight, dehydrated in 100% ethanol, and embedded in paraffin. 8 μm thick sections were used for hematoxylin eosin, Alcian blue and immunohistochemistry staining. *Klf2* in situ hybridization was performed as previously reported (Lee et al., 2006). The following antibodies were used for immunostaining: rat anti-Pecam (1:500, BD PharMingen), rabbit anti-Versican (1:200, Millipore), rabbit anti-DPEAAE (1:200, Pierce-Antibodies).

Zebrafish studies

Zebrafish were maintained and with approval of the Institutional Animal Care and Use Committee of the University of Pennsylvania. ccm2^{hi296} mutant zebrafish were obtained from the Zebrafish International Resource Center (ZIRC). *i-fabp*:GFP transgenic embryos in which the heart is fluorescently labeled were kindly provided by Dr. Michael Pack. The cardiac reporter zebrafish were created by transposon-based gene trap approach using the 192bp zebrafish I-FABP promoter (Her et al., 2004). Morpholino

oligonucleotides were obtained from Gene Tools (Philomath, OR) and were injected into the yolk of one-cell stage embryos at the indicated dosages and combinations. The morpholino sequences are described in Supplemental Experimental Procedures.

Biochemical studies.

Biochemical studies of E10.5 *Nfatc1*^{Cre};*Krit1*$^{fl/fl}$ hearts were performed as previously described (Kleaveland et al., 2009; Zheng et al., 2010). The following antibodies were used for immunonlotting: rabbit anti-Gapdh (1:5000, Cell Signaling), rabbit anti-pERK5 (1:1000, Cell Signaling), rabbit anti-Adamts5 (1:1000, Abcam), rabbit anti-DPEAAE (1:1000, Pierce-Antibodies). Identification of BirA-MEKK3 interacting proteins is described in Supplemental Materials and Methods.

Endothelial cell studies

Human umbilical vein endothelial cells (HUVEC; Lonza) were grown in EBM media supplemented with EGM-2 SingleQuots (Lonza). HUVECs were transfected overnight with 10nM Ambion Silencer Select siRNA against Map3k3 (s8671, Invitrogen) or Ccm2 (s8671, Invitrogen) using siPORT Amine Transfection Agent (Invitrogen) according to the manufacturer's protocol. 72 hours after transfection, total RNA was isolated using TRIzol Reagent (Invitrogen). cDNA was generated from 1 μg total RNA using Superscript III Reverse Transcriptase (Invitrogen). qPCR was performed in Power SYBR Green PCR Master Mix (Applied Biosciences) using primers described in Supplemental Materials and Methods.

Mouse heart explant studies

Hearts from wild type embryos on mixed background were collected at E10.5 and cultured in the presence of BIX02189 (5 uM) or DMSO for 24 h on transwell filters as described previously (Lavine et al., 2005).

Statistics

P values were calculated using an unpaired 2-tailed Student's t-test, ANOVA, or Chi Square analysis as indicated. The mean and standard error of mean (SEM) are shown in the bar graphs.

Author Contributions

ZZ and DR designed and performed most of the experiments and helped write the manuscript. SA, KW, DL, and BZ provided critical reagents. LG, WP, XC, ZJ, HZ, JY, XJ, BG and MK helped design and perform the experiments and wrote the manuscript.

Acknowledgements

We thank the members of the Kahn lab for their thoughtful comments during the course of this work. We thank Drs. Babette Weksler, Pierre-Olivier Couraud and Ignacio Romero for providing the hCMEC/D3 endothelial cells. These studies were supported by National Institute of Health grants R01HL094326 (MLK), R01HL102138 (MLK), R01NS075168 (KW), T32HL007971 (DR), and American Heart Association grant 11SDG7430025 (XZ).

References

Akers, A.L., Johnson, E., Steinberg, G.K., Zabramski, J.M., and Marchuk, D.A. (2009). Biallelic somatic and germline mutations in cerebral cavernous malformations (CCMs): evidence for a two-hit mechanism of CCM pathogenesis. Hum Mol Genet *18*, 919-930.

Boulday, G., Blecon, A., Petit, N., Chareyre, F., Garcia, L.A., Niwa-Kawakita, M., Giovannini, M., and Tournier-Lasserve, E. (2009). Tissue-specific conditional CCM2 knockout mice establish the essential role of endothelial CCM2 in angiogenesis: implications for human cerebral cavernous malformations. Dis Model Mech *2*, 168-177.

Boulday, G., Rudini, N., Maddaluno, L., Blecon, A., Arnould, M., Gaudric, A., Chapon, F., Adams, R.H., Dejana, E., and Tournier-Lasserve, E. (2011). Developmental timing of CCM2 loss influences cerebral cavernous malformations in mice. J Exp Med.

Bouwmeester, T., Bauch, A., Ruffner, H., Angrand, P.O., Bergamini, G., Croughton, K., Cruciat, C., Eberhard, D., Gagneur, J., Ghidelli, S.*, et al.* (2004). A physical and functional map of the human TNF-alpha/NF-kappa B signal transduction pathway. Nat Cell Biol *6*, 97-105.

Camenisch, T.D., Spicer, A.P., Brehm-Gibson, T., Biesterfeldt, J., Augustine, M.L., Calabro, A., Jr., Kubalak, S., Klewer, S.E., and McDonald, J.A. (2000). Disruption of hyaluronan synthase-2 abrogates normal cardiac morphogenesis and hyaluronan-mediated transformation of epithelium to mesenchyme. J Clin Invest *106*, 349-360.

Chan, A.C., Drakos, S.G., Ruiz, O.E., Smith, A.C., Gibson, C.C., Ling, J., Passi, S.F., Stratman, A.N., Sacharidou, A., Revelo, M.P.*, et al.* (2011). Mutations in 2 distinct genetic pathways result in cerebral cavernous malformations in mice. J Clin Invest *121*, 1871-1881.

Chan, A.C., Li, D.Y., Berg, M.J., and Whitehead, K.J. (2010). Recent insights into cerebral cavernous malformations: animal models of CCM and the human phenotype. FEBS J *277*, 1076-1083.

Chao, T.H., Hayashi, M., Tapping, R.I., Kato, Y., and Lee, J.D. (1999). MEKK3 directly regulates MEK5 activity as part of the big mitogen-activated protein kinase 1 (BMK1) signaling pathway. J Biol Chem *274*, 36035-36038.

Deacon, K., and Blank, J.L. (1999). MEK kinase 3 directly activates MKK6 and MKK7, specific activators of the p38 and c-Jun NH2-terminal kinases. J Biol Chem *274*, 16604-16610.

Dekker, R.J., Boon, R.A., Rondaij, M.G., Kragt, A., Volger, O.L., Elderkamp, Y.W., Meijers, J.C., Voorberg, J., Pannekoek, H., and Horrevoets, A.J. (2006). KLF2 provokes a gene expression pattern that establishes functional quiescent differentiation of the endothelium. Blood.

Dekker, R.J., van Soest, S., Fontijn, R.D., Salamanca, S., de Groot, P.G., VanBavel, E., Pannekoek, H., and Horrevoets, A.J. (2002). Prolonged fluid shear stress induces a distinct set of endothelial cell genes, most specifically lung Kruppel-like factor (KLF2). Blood *100*, 1689-1698.

Dupuis, L.E., McCulloch, D.R., McGarity, J.D., Bahan, A., Wessels, A., Weber, D., Diminich, A.M., Nelson, C.M., Apte, S.S., and Kern, C.B. (2011). Altered versican cleavage in ADAMTS5 deficient mice; a novel etiology of myxomatous valve disease. Dev Biol *357*, 152-164.

Gassmann, M., Casagranda, F., Orioli, D., Simon, H., Lai, C., Klein, R., and Lemke, G. (1995). Aberrant neural and cardiac development in mice lacking the ErbB4 neuregulin receptor. Nature *378*, 390-394.

Glading, A., Han, J., Stockton, R.A., and Ginsberg, M.H. (2007). KRIT-1/CCM1 is a Rap1 effector that regulates endothelial cell cell junctions. J Cell Biol *179*, 247-254.
Grego-Bessa, J., Luna-Zurita, L., del Monte, G., Bolos, V., Melgar, P., Arandilla, A.,

Garratt, A.N., Zang, H., Mukouyama, Y.S., Chen, H.*, et al.* (2007). Notch signaling is essential for ventricular chamber development. Dev Cell *12*, 415-429.

Groenendijk, B.C., Hierck, B.P., Vrolijk, J., Baiker, M., Pourquie, M.J., Gittenberger-de Groot, A.C., and Poelmann, R.E. (2005). Changes in shear stress-related gene expression after experimentally altered venous return in the chicken embryo. Circ Res *96*, 1291-1298.

Hale, A.T., Tian, H., Anih, E., Recio, F.O., 3rd, Shatat, M.A., Johnson, T., Liao, X., Ramirez-Bergeron, D.L., Proweller, A., Ishikawa, M.*, et al.* (2014). Endothelial Kruppel-like factor 4 regulates angiogenesis and the Notch signaling pathway. J Biol Chem *289*, 12016-12028.

Her, G.M., Chiang, C.C., and Wu, J.L. (2004). Zebrafish intestinal fatty acid binding protein (I-FABP) gene promoter drives gut-specific expression in stable transgenic fish. Genesis *38*, 26-31.

Hilder, T.L., Malone, M.H., Bencharit, S., Colicelli, J., Haystead, T.A., Johnson, G.L., and Wu, C.C. (2007). Proteomic identification of the cerebral cavernous malformation signaling complex. J Proteome Res *6*, 4343-4355.

Huddleson, J.P., Srinivasan, S., Ahmad, N., and Lingrel, J.B. (2004). Fluid shear stress induces endothelial KLF2 gene expression through a defined promoter region. Biol Chem *385*, 723-729.

Jeansson, M., Gawlik, A., Anderson, G., Li, C., Kerjaschki, D., Henkelman, M., and Quaggin, S.E. (2011). Angiopoietin-1 is essential in mouse vasculature during development and in response to injury. J Clin Invest *121*, 2278-2289.

Jenni, R., Rojas, J., and Oechslin, E. (1999). Isolated noncompaction of the myocardium. N Engl J Med *340*, 966-967.

Kleaveland, B., Zheng, X., Liu, J.J., Blum, Y., Tung, J.J., Zou, Z., Sweeney, S.M., Chen, M., Guo, L., Lu, M.M.*, et al.* (2009). Regulation of cardiovascular development and integrity by the heart of glass-cerebral cavernous malformation protein pathway. Nat Med *15*, 169-176.

Kuo, C.T., Veselits, M.L., Barton, K.P., Lu, M.M., Clendenin, C., and Leiden, J.M. (1997). The LKLF transcription factor is required for normal tunica media formation and blood vessel stabilization during murine embryogenesis. Genes Dev *11*, 2996-3006.

Lavine, K.J., Yu, K., White, A.C., Zhang, X., Smith, C., Partanen, J., and Ornitz, D.M. (2005). Endocardial and epicardial derived FGF signals regulate myocardial proliferation and differentiation in vivo. Dev Cell *8*, 85-95.

Lee, J.S., Yu, Q., Shin, J.T., Sebzda, E., Bertozzi, C., Chen, M., Mericko, P., Stadtfeld, M., Zhou, D., Cheng, L.*, et al.* (2006). Klf2 is an essential regulator of vascular hemodynamic forces in vivo. Dev Cell *11*, 845-857.

Li, D.Y., and Whitehead, K.J. (2010). Evaluating strategies for the treatment of cerebral cavernous malformations. Stroke *41*, S92-94.

Li, L., Tatake, R.J., Natarajan, K., Taba, Y., Garin, G., Tai, C., Leung, E., Surapisitchat, J., Yoshizumi, M., Yan, C.*, et al.* (2008). Fluid shear stress inhibits TNF-mediated JNK activation via MEK5-BMK1 in endothelial cells. Biochem Biophys Res Commun *370*, 159-163.

Liu, W., Draheim, K.M., Zhang, R., Calderwood, D.A., and Boggon, T.J. (2013). Mechanism for KRIT1 release of ICAP1-mediated suppression of integrin activation. Mol Cell *49*, 719-729.

Mably, J.D., Chuang, L.P., Serluca, F.C., Mohideen, M.A., Chen, J.N., and Fishman, M.C. (2006). santa and valentine pattern concentric growth of cardiac myocardium in the zebrafish. Development *133*, 3139-3146.

Mably, J.D., Mohideen, M.A., Burns, C.G., Chen, J.N., and Fishman, M.C. (2003). heart of glass regulates the concentric growth of the heart in zebrafish. Curr Biol *13*, 2138-2147.

Maddaluno, L., Rudini, N., Cuttano, R., Bravi, L., Giampietro, C., Corada, M., Ferrarini, L., Orsenigo, F., Papa, E., Boulday, G., *et al.* (2013). EndMT contributes to the onset and progression of cerebral cavernous malformations. Nature *498*, 492-496.

McDonald, D.A., Shenkar, R., Shi, C., Stockton, R.A., Akers, A.L., Kucherlapati, M.H., Kucherlapati, R., Brainer, J., Ginsberg, M.H., Awad, I.A., *et al.* (2011). A novel mouse model of cerebral cavernous malformations based on the two-hit mutation hypothesis recapitulates the human disease. Hum Mol Genet *20*, 211-222.

McDonald, D.A., Shi, C., Shenkar, R., Stockton, R.A., Liu, F., Ginsberg, M.H., Marchuk, D.A., and Awad, I.A. (2012). Fasudil decreases lesion burden in a murine model of cerebral cavernous malformation disease. Stroke *43*, 571-574.

Mleynek, T.M., Chan, A., Redd, M., Gibson, C.C., Davis, C., Shi, D.S., Chen, T., Carter, K.L., Ling, J., Blanco, R., *et al.* (2014). Lack of CCM1 Induces Hypersprouting and Impairs Response to Flow. Hum Mol Genet.

Nakamura, A., and Manasek, F.J. (1981). An experimental study of the relation of cardiac jelly to the shape of the early chick embryonic heart. J Embryol Exp Morphol *65*, 235-256.

Nakamura, K., and Johnson, G.L. (2003). PB1 domains of MEKK2 and MEKK3 interact with the MEK5 PB1 domain for activation of the ERK5 pathway. J Biol Chem *278*, 36989-36992.

Nebreda, A.R., and Porras, A. (2000). p38 MAP kinases: beyond the stress response. Trends Biochem Sci *25*, 257-260.

Parmar, K.M., Larman, H.B., Dai, G., Zhang, Y., Wang, E.T., Moorthy, S.N., Kratz, J.R., Lin, Z., Jain, M.K., Gimbrone, M.A., *et al.* (2006). Integration of flow-dependent endothelial phenotypes by Kruppel-like factor 2. J Clin Invest *116*, 49-58.

Parmar, K.M., Nambudiri, V., Dai, G., Larman, H.B., Gimbrone, M.A., Jr., and Garcia-Cardena, G. (2005). Statins exert endothelial atheroprotective effects via the KLF2 transcription factor. J Biol Chem *280*, 26714-26719.

Riant, F., Bergametti, F., Ayrignac, X., Boulday, G., and Tournier-Lasserve, E. (2010). Recent insights into cerebral cavernous malformations: the molecular genetics of CCM. FEBS J *277*, 1070-1075.

Roux, K.J., Kim, D.I., Raida, M., and Burke, B. (2012). A promiscuous biotin ligase fusion protein identifies proximal and interacting proteins in mammalian cells. J Cell Biol *196*, 801-810.

Sandy, J.D., Westling, J., Kenagy, R.D., Iruela-Arispe, M.L., Verscharen, C., Rodriguez-Mazaneque, J.C., Zimmermann, D.R., Lemire, J.M., Fischer, J.W., Wight, T.N., *et al.*

(2001). Versican V1 proteolysis in human aorta in vivo occurs at the Glu441-Ala442 bond, a site that is cleaved by recombinant ADAMTS-1 and ADAMTS-4. J Biol Chem *276*, 13372-13378.

Serebriiskii, I., Estojak, J., Sonoda, G., Testa, J.R., and Golemis, E.A. (1997). Association of Krev-1/rap1a with Krit1, a novel ankyrin repeat-containing protein encoded by a gene mapping to 7q21-22. Oncogene *15*, 1043-1049.

Sohn, S.J., Li, D., Lee, L.K., and Winoto, A. (2005). Transcriptional regulation of tissue-specific genes by the ERK5 mitogen-activated protein kinase. Mol Cell Biol *25*, 8553-8566.

Somekawa, S., Imagawa, K., Hayashi, H., Sakabe, M., Ioka, T., Sato, G.E., Inada, K., Iwamoto, T., Mori, T., Uemura, S.*, et al.* (2012). Tmem100, an ALK1 receptor signaling-dependent gene essential for arterial endothelium differentiation and vascular morphogenesis. Proc Natl Acad Sci U S A *109*, 12064-12069.

Stankunas, K., Hang, C.T., Tsun, Z.Y., Chen, H., Lee, N.V., Wu, J.I., Shang, C., Bayle, J.H., Shou, W., Iruela-Arispe, M.L.*, et al.* (2008). Endocardial Brg1 represses ADAMTS1 to maintain the microenvironment for myocardial morphogenesis. Dev Cell *14*, 298-311.

Stockton, R.A., Shenkar, R., Awad, I.A., and Ginsberg, M.H. (2010). Cerebral cavernous malformations proteins inhibit Rho kinase to stabilize vascular integrity. J Exp Med.

Tatake, R.J., O'Neill, M.M., Kennedy, C.A., Wayne, A.L., Jakes, S., Wu, D., Kugler, S.Z., Jr., Kashem, M.A., Kaplita, P., and Snow, R.J. (2008). Identification of pharmacological inhibitors of the MEK5/ERK5 pathway. Biochem Biophys Res Commun *377*, 120-125.

Uhlik, M.T., Abell, A.N., Johnson, N.L., Sun, W., Cuevas, B.D., Lobel-Rice, K.E., Horne, E.A., Dell'Acqua, M.L., and Johnson, G.L. (2003). Rac-MEKK3-MKK3 scaffolding for p38 MAPK activation during hyperosmotic shock. Nat Cell Biol *5*, 1104-1110.

Vermot, J., Forouhar, A.S., Liebling, M., Wu, D., Plummer, D., Gharib, M., and Fraser, S.E. (2009). Reversing blood flows act through klf2a to ensure normal valvulogenesis in the developing heart. PLoS Biol *7*, e1000246.

Villarreal, G., Jr., Zhang, Y., Larman, H.B., Gracia-Sancho, J., Koo, A., and Garcia-Cardena, G. (2010). Defining the regulation of KLF4 expression and its downstream transcriptional targets in vascular endothelial cells. Biochem Biophys Res Commun *391*, 984-989.

Weksler, B.B., Subileau, E.A., Perriere, N., Charneau, P., Holloway, K., Leveque, M., Tricoire-Leignel, H., Nicotra, A., Bourdoulous, S., Turowski, P.*, et al.* (2005). Blood-

brain barrier-specific properties of a human adult brain endothelial cell line. Faseb J *19*, 1872-1874.

Whitehead, K.J., Chan, A.C., Navankasattusas, S., Koh, W., London, N.R., Ling, J., Mayo, A.H., Drakos, S.G., Jones, C.A., Zhu, W.*, et al.* (2009). The cerebral cavernous malformation signaling pathway promotes vascular integrity via Rho GTPases. Nat Med *15*, 177-184.

Whitehead, K.J., Plummer, N.W., Adams, J.A., Marchuk, D.A., and Li, D.Y. (2004). Ccm1 is required for arterial morphogenesis: implications for the etiology of human cavernous malformations. Development *131*, 1437-1448.

Wu, B., Zhang, Z., Lui, W., Chen, X., Wang, Y., Chamberlain, A.A., Moreno-Rodriguez, R.A., Markwald, R.R., O'Rourke, B.P., Sharp, D.J.*, et al.* (2012). Endocardial cells form the coronary arteries by angiogenesis through myocardial-endocardial VEGF signaling. Cell *151*, 1083-1096.

Yamamura, H., Zhang, M., Markwald, R.R., and Mjaatvedt, C.H. (1997). A heart segmental defect in the anterior-posterior axis of a transgenic mutant mouse. Dev Biol *186*, 58-72.

Yang, J., Boerm, M., McCarty, M., Bucana, C., Fidler, I.J., Zhuang, Y., and Su, B. (2000). Mekk3 is essential for early embryonic cardiovascular development. Nat Genet *24*, 309-313.

Zawistowski, J.S., Stalheim, L., Uhlik, M.T., Abell, A.N., Ancrile, B.B., Johnson, G.L., and Marchuk, D.A. (2005). CCM1 and CCM2 protein interactions in cell signaling: implications for cerebral cavernous malformations pathogenesis. Hum Mol Genet *14*, 2521-2531.

Zhang, J., Rigamonti, D., Dietz, H.C., and Clatterbuck, R.E. (2007). Interaction between krit1 and malcavernin: implications for the pathogenesis of cerebral cavernous malformations. Neurosurgery *60*, 353-359; discussion 359.

Zheng, X., Xu, C., Di Lorenzo, A., Kleaveland, B., Zou, Z., Seiler, C., Chen, M., Cheng, L., Xiao, J., He, J.*, et al.* (2010). CCM3 signaling through sterile 20-like kinases plays an essential role during zebrafish cardiovascular development and cerebral cavernous malformations. J Clin Invest *120*, 2795-2804.

Zheng, X., Xu, C., Smith, A.O., Stratman, A.N., Zou, Z., Kleaveland, B., Yuan, L., Didiku, C., Sen, A., Liu, X.*, et al.* (2012). Dynamic regulation of the cerebral cavernous malformation pathway controls vascular stability and growth. Dev Cell *23*, 342-355.

Figure Legends

Figure 1. Lack of endocardial *Krit1* results in loss of cardiac jelly. A-D. *Nfatc1*^{Cre}*;Krit1*$^{fl/fl}$ hearts exhibit thinned myocardium and reduced space between endocardial and myocardial cells at E10.5 and E12.5. Arrows indicate the endocardial-myocardial gap. A'-D' show higher magnification images of the regions boxed in A-D. **E.** Ratio of the area occupied by cardiac jelly to that occupied by myocardium in the trabeculae of E10.5 littermate hearts. N=3 embryos; 9 sections analyzed for each group. ** indicates P<0.01. **F, G.** Reduced Alcian blue staining in *Nfatc1*^{Cre}*;Krit1*$^{fl/fl}$ hearts at E10.5. F' and G' show higher magnification images of the regions boxed in F and G. **H, I.** Immunostaining for versican in *Nfatc1*^{Cre}*;Krit1*$^{fl/fl}$ and control hearts at E10.5. H' and I' show higher magnification images of the regions boxed in H and I. Scale bars indicate 100 μm.

Figure 2. Endocardial loss of *Ccm2* or *Pdcd10* also results in reduced cardiac jelly. **A, B.** Thin myocardium and reduced endocardial-myocardial space in *Nfatc1*^{Cre}*;Ccm2*$^{fl/fl}$ hearts at E10.5. A' and B' show higher magnification images of the regions boxed in A and B. **C, D.** Reduced Alcian blue staining in *Nfatc1*^{Cre}*;Ccm2*$^{fl/fl}$ hearts at E10.5. **E, F.** Reduced intact versican in in *Nfatc1*^{Cre}*;Ccm2*$^{fl/fl}$ hearts at E10.5. **G, H.** Thin myocardium and reduced endocardial-myocardial space in *Nfatc1*^{Cre}*;Ccm2*$^{fl/fl}$ hearts at E12.5. G' and H' show higher magnification images of the regions boxed in G and H. **I, J.** Reduced Alcian blue staining in *Nfatc1*^{Cre}*;Ccm2*$^{fl/fl}$ hearts at E12.5. **K, L.** Reduced intact versican in in *Nfatc1*^{Cre}*;Ccm2*$^{fl/fl}$ hearts at E12.5. **M, N.** Thin myocardium and reduced

endocardial-myocardial space in *Nfatc1*^{Cre};*Pdcd10*$^{fl/fl}$ hearts at E12.5. M' and N' show higher magnification images of the regions boxed in M and N. **O, P.** Reduced Alcian blue staining in *Nfatc1*^{Cre}; *Pdcd10*$^{fl/fl}$ hearts at E12.5. **Q, R.** Reduced intact versican in in *Nfatc1*^{Cre}; *Pdcd10*$^{fl/fl}$ hearts at E12.5. Scale bars indicate 100 μm.

Figure 3. Loss of CCM signaling results in increased *Klf2* and *Adamts5* expression and function. A. Microarray analysis of mRNA expression in E10.5 *Nfatc1*^{Cre};*Krit1*$^{fl/fl}$ and *Krit1*$^{fl/+}$ littermate hearts reveals increased levels of *Klf2*, *Klf4,* KLF2 target genes and *Adamts5*, and reduced levels of *Dll4* and *Tmem100*. N= 4 for both genotypes. **B.** qPCR of E10.5 hearts reveals preserved or increased expression of *Nrg1* and FGF growth factors following endocardial *Krit1* loss. **C.** qPCR of E10.5 hearts reveals elevated levels of *Klf2* and established KLF2 target genes following endocardial *Krit1* loss. **D.** qPCR analysis of genes associated with cardiac jelly matrix proteins and matrix-degrading proteases in E10.5 hearts reveals elevated levels of *Adamts5* following endocardial *Krit1* loss. N= 3 for *Krit1*$^{fl/fl}$, N= 4 for *Nfatc1*^{Cre};*Krit1*$^{fl/+}$, N=5 for *Nfatc1*^{Cre};*Krit1*$^{fl/fl}$ in B-D. **E.** In situ hybridization for *Klf2* in E10.5 *Nfatc1*^{Cre};*Krit1*$^{fl/fl}$ and *Krit1*$^{fl/fl}$ littermate hearts. **F.** Immunostaining for KLF4 protein (arrows) and myocardium (MF20) in E10.5 *Nfatc1*^{Cre};*Krit1*$^{fl/fl}$ and *Krit1*$^{fl/fl}$ littermate hearts. **G.** Immunoblot analysis of KLF2 protein in whole E10.5 *Nfatc1*^{Cre};*Krit1*$^{fl/fl}$ and *Nfatc1*^{Cre};*Krit1*$^{fl/+}$ and *Krit1*$^{fl/fl}$ littermate hearts.. GAPDH is shown as a loading control. **H.** Immunostaining using anti-DPEAAE antibody to detect ADAMTS-cleaved versican reveals increased levels in the E10.5 *Nfatc1*^{Cre};*Krit1*$^{fl/fl}$ heart. Boxed regions are shown at higher magnification on the right. **I.** Immunoblot analysis of lysate derived from whole E10.5 hearts reveals increased levels

of cleaved versican (DPEAAE) and the ADAMTS5 protease with endocardial loss of *Krit1*. GAPDH is shown as a loading control. Scale bars indicate 100 μm. * indicates P <0.05; ** indicates P<0.01; *** indicates P<0.001.

Figure 4. Loss of *klf2* or *adamts5* rescues the cardiac phenotype conferred by loss of CCM signaling in zebrafish embryos. A-C. H-E and Alcian blue staining of adjacent sections from a 72 hpf control zebrafish heart reveal a myocardial wall with multiple cell layers (A) and the presence of Alcian blue-staining cardiac jelly (B, C). **D-F.** H-E and Alcian blue staining of adjacent sections from a 72 hpf *ccm2* mutant heart reveals a thin myocardial wall (D) and lack of cardiac jelly (E, F). C and F are higher magnification images of the boxed regions in B and E respectively. **G.** Injection of zebrafish embryos with *krit1* morpholinos results in a big heart at 72 hpf detected by light microscopy and in *i-fabp*:GFP transgenic embryos in which the heart is fluorescently labeled. **H.** Injection of morpholinos targeting both *krit1* and the two *klf2* zebrafish orthologues rescues the big heart phenotype at 72 hpf. **I.** Injection of morpholinos targeting both *krit1* and *adamts5* rescues the big heart phenotype at 72 hpf. **J.** Efficiency of rescue of the *krit1* morphant heart phenotype with *klf2* and *adamts5* morpholinos. *** indicates P<0.001. **K.** Knockdown of *klf2* or *adamts5* also rescues the cardiac phenotype in *ccm2* mutant zebrafish embryos. The frequency of a big heart phenotype in the offspring of $ccm2^{+/-}$ intercrosses treated with control, *klf2* or *adamts5* morpholinos is shown. ** indicates P<0.01; * indicates P<0.05. The number of total embryos analyzed and number experimental repeats (in parenthesis) in J and K are indicated above each bar. Scale bars indicate 100 μm.

Figure 5. MEKK3 regulates expression of *KLF* and *ADAMTS* genes in cultured endothelial cells and in the endocardium of the developing heart. **A.** Tetracycline-regulated expression of BirA-MEKK3 drives dose-dependent expression of *KLF2* and *KLF4* in HUVEC. **B.** siRNA knockdown of *MEKK3* in HUVEC blocks flow-induced expression of *KLF2, KLF4* and *ADAMTS4.* HUVEC were exposed to 16 hours of laminar shear after exposure to siRNA directed against *MEKK3 (MAP3K3)* or control, scrambled siRNA. N=5; P<0.0001. **C.** qPCR of E10.5 hearts reveals severely reduced levels of *Klf2, Klf4* and known KLF2/4 target genes following endocardial *Mekk3* (*Map3k3)* deletion. N= 3 for all groups. **D.** qPCR of E10.5 hearts reveals reduced levels of *Nrg1* and *Adamts5* but normal levels of FGFs following endocardial *Mekk3* (*Map3k3)* deletion. N= 3 for all groups. **E.** qPCR of E9.5 wild-type mouse hearts following 24 hour incubation in medium containing the MEK5 inhibitor BIX02188 ("BIX") or DMSO ("control"). N= 3 for all groups. * indicates P <0.05; ** indicates P<0.01; *** indicates P<0.001; **** indicates P<0.0001.

Figure 6. Loss of MEKK3 rescues the CCM-deficient phenotype in cultured endothelial cells and zebrafish embryos.

A. siRNA knockdown of CCM2 increases the level of phospho-ERK5 in cultured HUVEC. **B-D.** siRNA knockdown of CCM2 increases the expression of *KLF2, KLF4* and *ADAMTS4* in HUVEC, and these changes in gene expression are reversed by siRNA knockdown of *MEKK3 (MAP3K3)*. **E, F.** Injection of zebrafish embryos with *krit1* morpholinos results in a big heart at 72 hpf in *i-fabp*:GFP transgenic embryos in which

the heart is fluorescently labeled. **G.** Injection of morpholinos targeting both *krit1* and *map3k3* rescues the big heart phenotype at 72 hpf. **H.** Efficiency of rescue of the *krit1* morphant heart phenotype with *map3k3* morpholinos. *** indicates P<0.001. **I.** Knockdown of *map3k3* rescues the cardiac phenotype in *ccm2* mutant zebrafish embryos. The frequency of a big heart phenotype in the offspring of $ccm2^{+/-}$ intercrosses treated with control or *map3k3* morpholinos is shown. *** indicates P<0.001. The number of total embryos analyzed and number experimental repeats (in parenthesis) are indicated above each bar in H and I . Scale bars indicate 100 μm.

Figure 7. Reduced *Mekk3* expression rescues the loss of cardiac jelly and changes in gene expression conferred by endocardial loss of *Krit1*.

A-C. The endocardial-myocardial space occupied by cardiac jelly is increased in $Nfatc1^{Cre};Krit1^{fl/fl};Map3k3^{fl/+}$ hearts compared with $Nfatc1^{Cre};Krit1^{fl/fl};Map3k3^{+/+}$ littermates at E10.5. Higher magnification images of the boxed regions are shown on the right. **D-F.** Alcian blue staining for cardiac jelly is increased in $Nfatc1^{Cre};Krit1^{fl/fl};Map3k3^{fl/+}$ hearts compared with $Nfatc1^{Cre};Krit1^{fl/fl};Map3k3^{+/+}$ littermates at E10.5. **G-I.** Versican in cardiac jelly is increased in $Nfatc1^{Cre};Krit1^{fl/fl};Map3k3^{fl/+}$ hearts compared with $Nfatc1^{Cre};Krit1^{fl/fl};Map3k3^{+/+}$ littermates at E10.5. **J.** The ratio of the area occupied by cardiac jelly to that occupied by myocardium in the trabeculae is increased in E10.5 $Nfatc1^{Cre};Krit1^{fl/fl};Map3k3^{fl/+}$ hearts compared with $Nfatc1^{Cre};Krit1^{fl/fl};Map3k3^{+/+}$ littermates. N=3 embryos; 9 sections analyzed for each group. **K.** Immunoblot analysis of lysate derived from whole E10.5 hearts reveals higher levels of cleaved versican (DPEAAE) in

Nfatc1^{Cre};*Krit1*$^{fl/fl}$;*Map3k3*$^{+/+}$ hearts compared with *Nfatc1*^{Cre};*Krit1*$^{fl/fl}$;*Map3k3*$^{fl/+}$ littermates. GAPDH is shown as a loading control. **L-N.** qPCR of E10.5 hearts reveals normalized expression of *Klf2, Klf4,* KLF2/4 target genes, *Nrg1, Dll4, Tmem100, Adamts4* and *Adamts5* in *Nfatc1*^{Cre};*Krit1*$^{fl/fl}$;*Map3k3*$^{fl/+}$ hearts compared with *Nfatc1*^{Cre};*Krit1*$^{fl/fl}$;*Map3k3*$^{+/+}$ littermates at E10.5. * indicates P <0.05; ** indicates P<0.01; *** indicates P<0.001. Scale bars indicate 100 μm. **O.** CCM regulation of MEKK3 activity and gene expression. The CCM complex binds MEKK3 through interaction with CCM2 and blocks MEKK3 signaling (left). Loss of the CCM complex increases MEKK3-ERK5 signaling and the expression of *Klf2* and *Adamts5*, resulting in the breakdown of cardiac jelly and reduced myocardial proliferation (right).

Figure 1

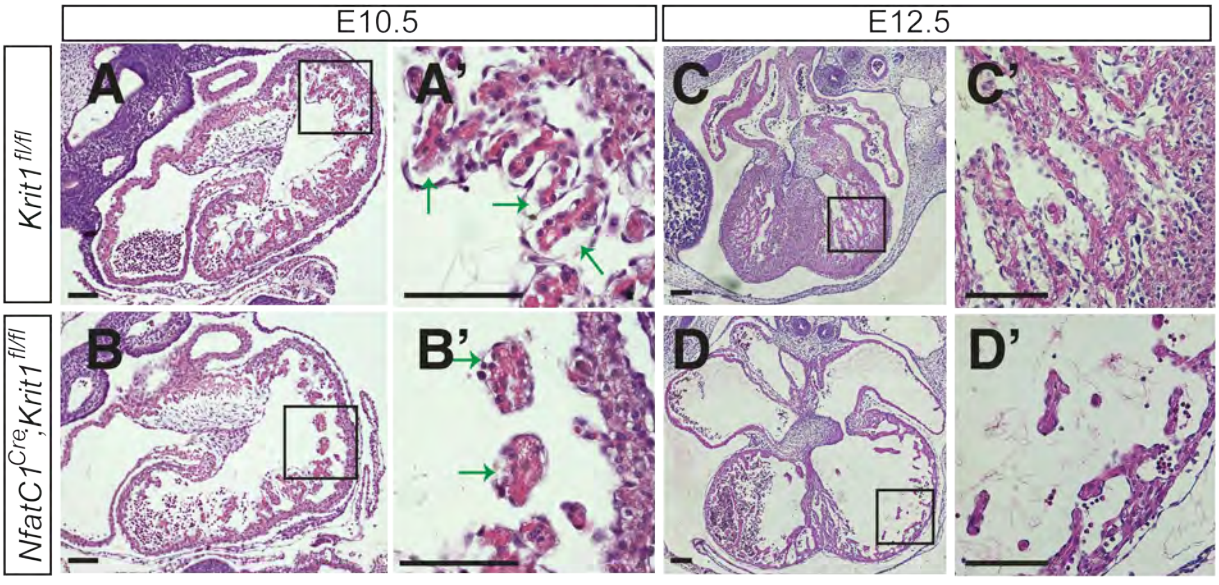
E10.5
E12.5
Krit1 fl/fl
NfatC1Cre;Krit1 fl/fl
A
A'
B
B'
C
C'
D
D'

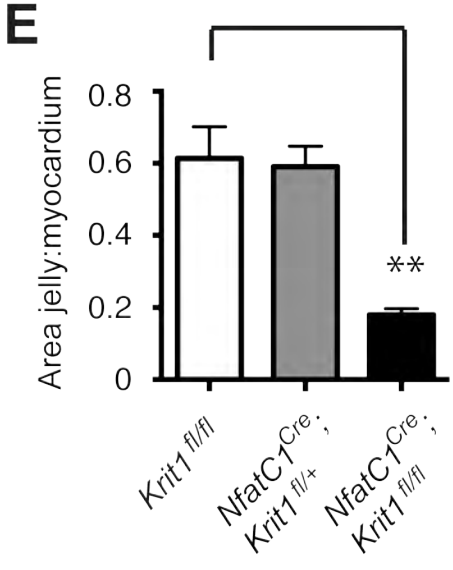
E
Area jelly:myocardium
0.8
0.6
0.4
0.2
0
**
Krit1 fl/fl
NfatC1Cre; Krit1 fl/+
NfatC1Cre; Krit1 fl/fl

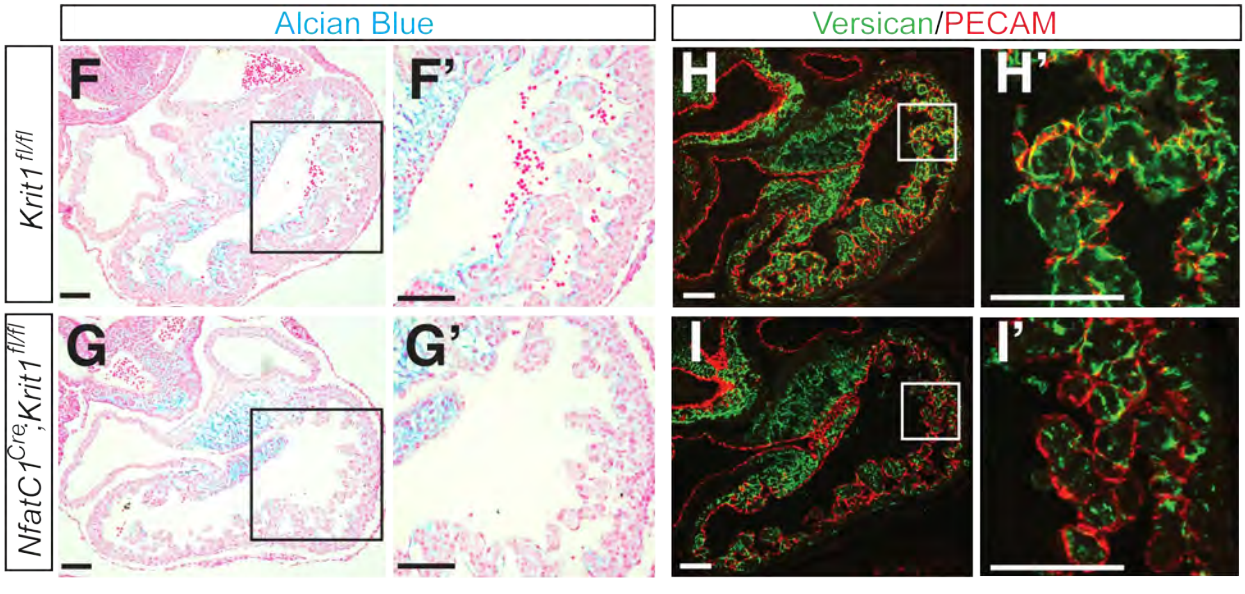
Alcian Blue
Versican/PECAM
Krit1 fl/fl
NfatC1Cre;Krit1 fl/fl
F
F'
G
G'
H
H'
I
I'

Figure 2

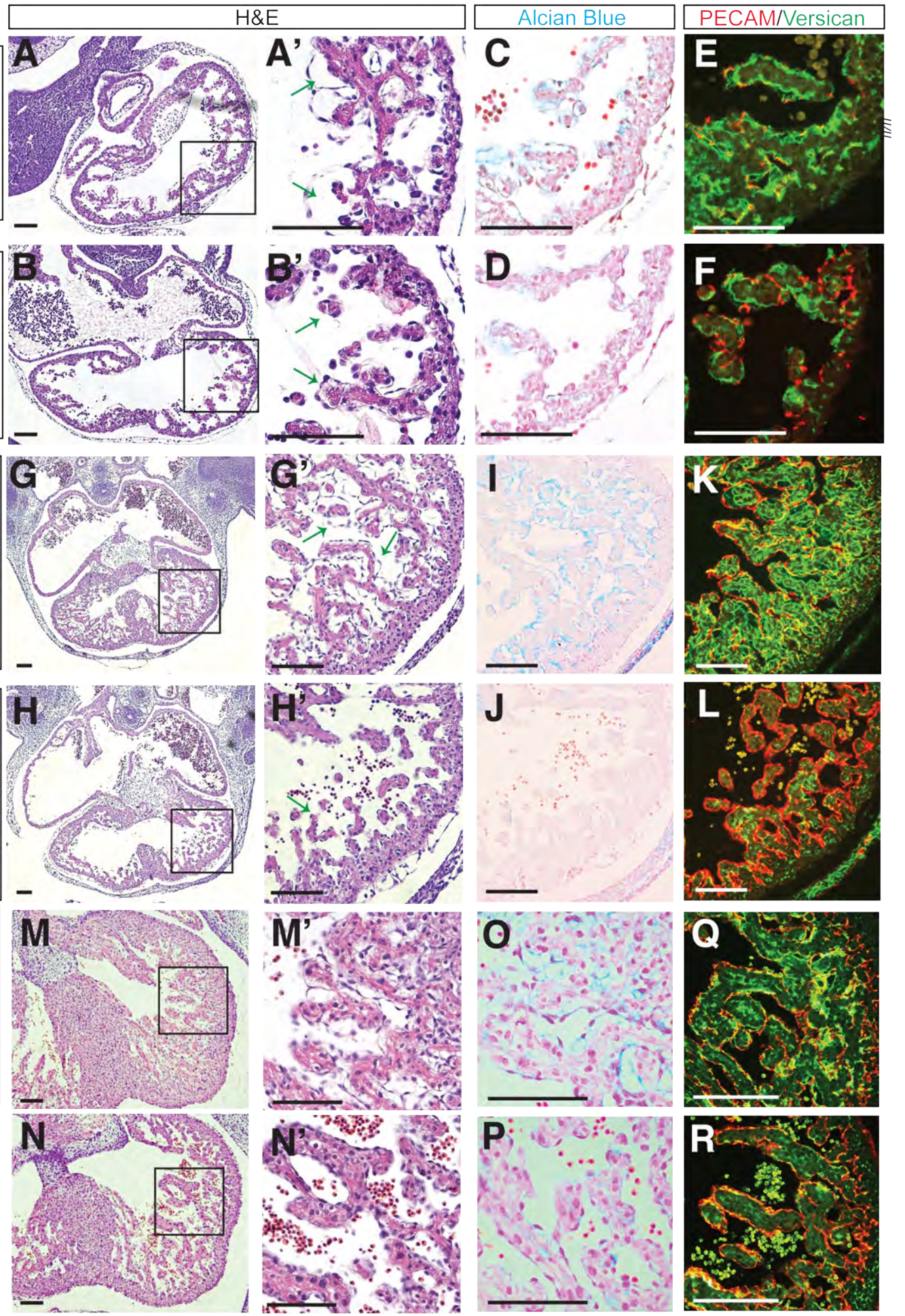
H&E
Alcian Blue
PECAM/Versican
Ccm2fl/fl
NfatC1Cre;Ccm2fl/fl
Ccm2fl/fl
NfatC1Cre;Ccm2fl/fl
NfatC1Cre;Pdcd10fl/+
NfatC1Cre;Pdcd10fl/-
A
A'
C
E
B
B'
D
F
G
G'
I
K
H
H'
J
L
M
M'
O
Q
N
N'
P
R

Figure 3

Figure 3

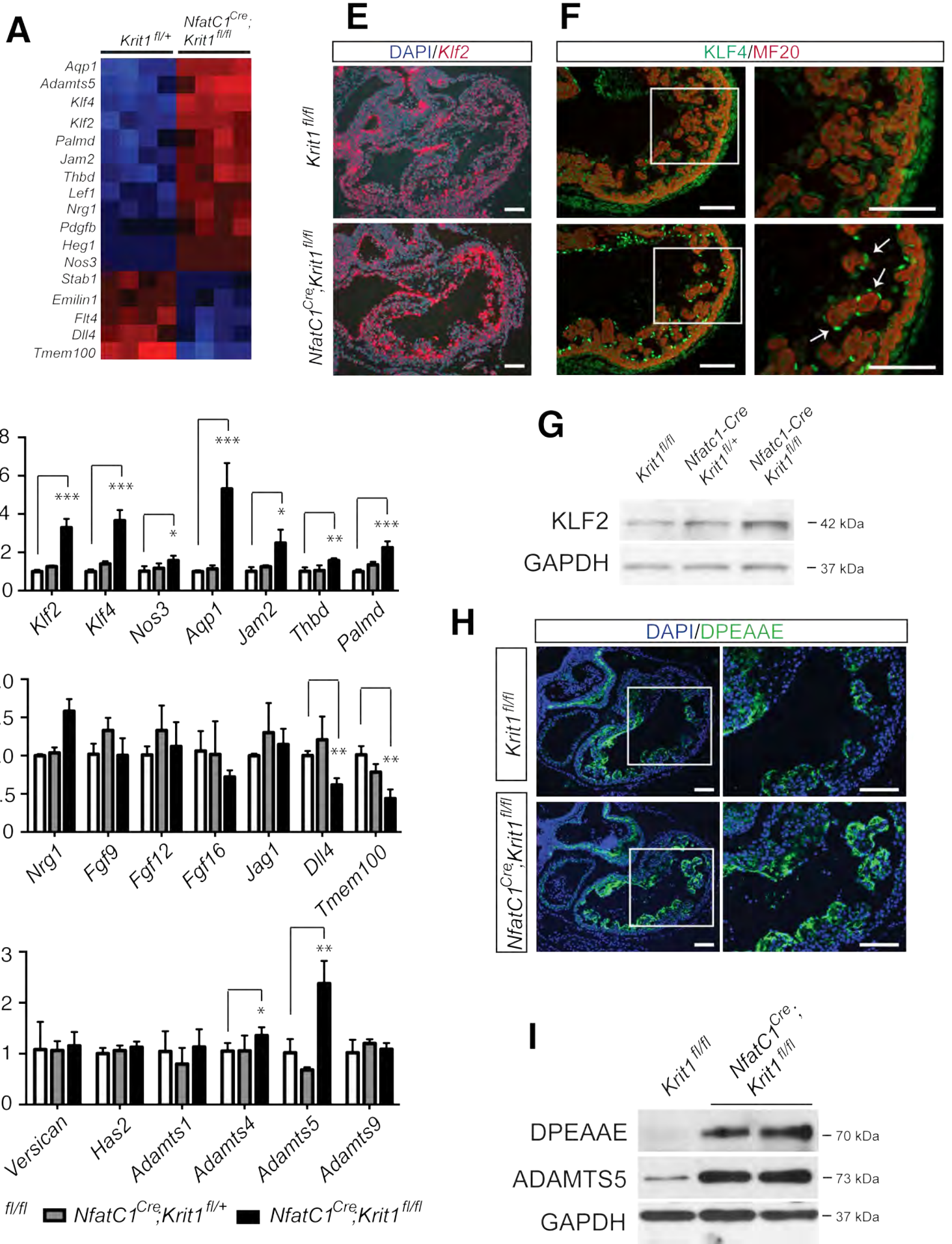

Figure 4

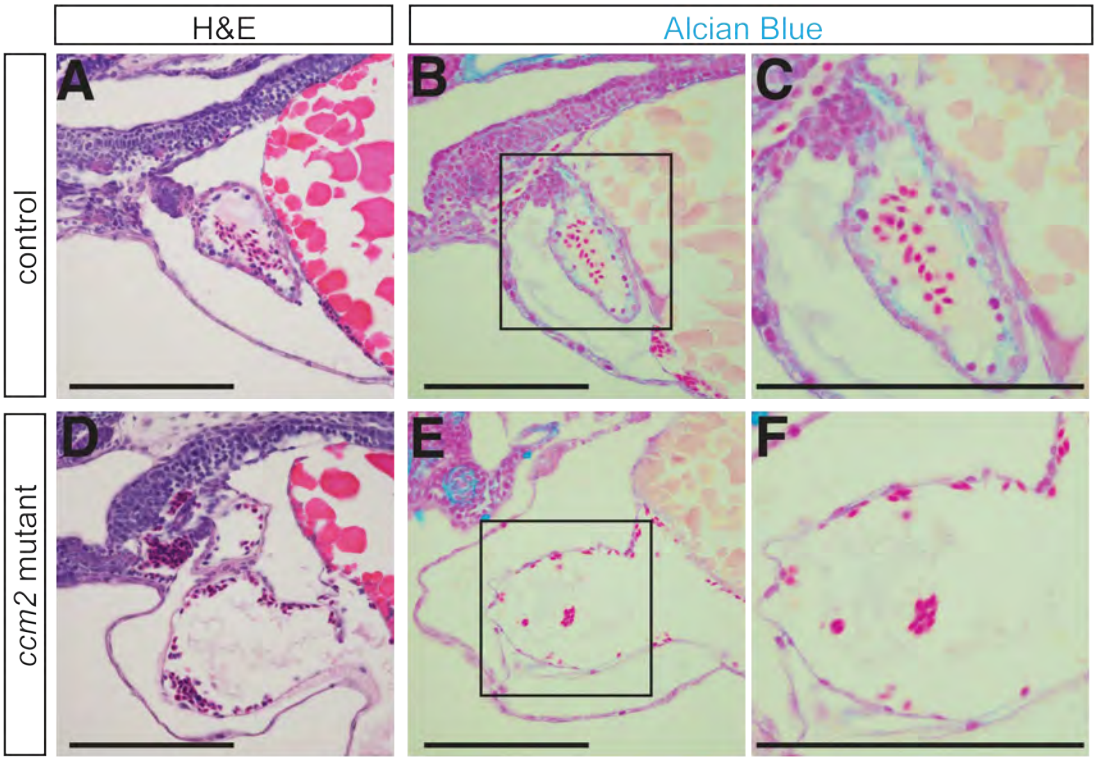
H&E
Alcian Blue
control
ccm2 mutant
A
B
C
D
E
F

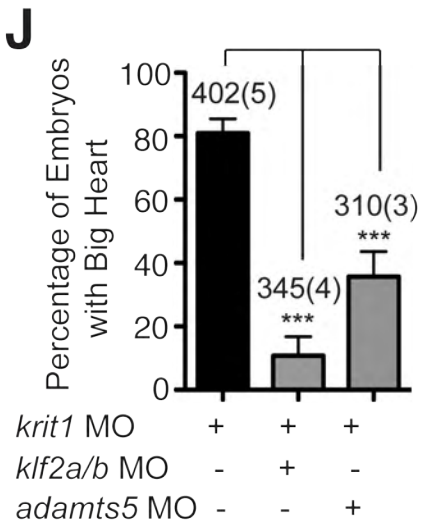
J
Percentage of Embryos with Big Heart
100
80
60
40
20
0
402(5)
345(4)
***
310(3)
***
krit1 MO + + +
klf2a/b MO - + -
adamts5 MO - - +

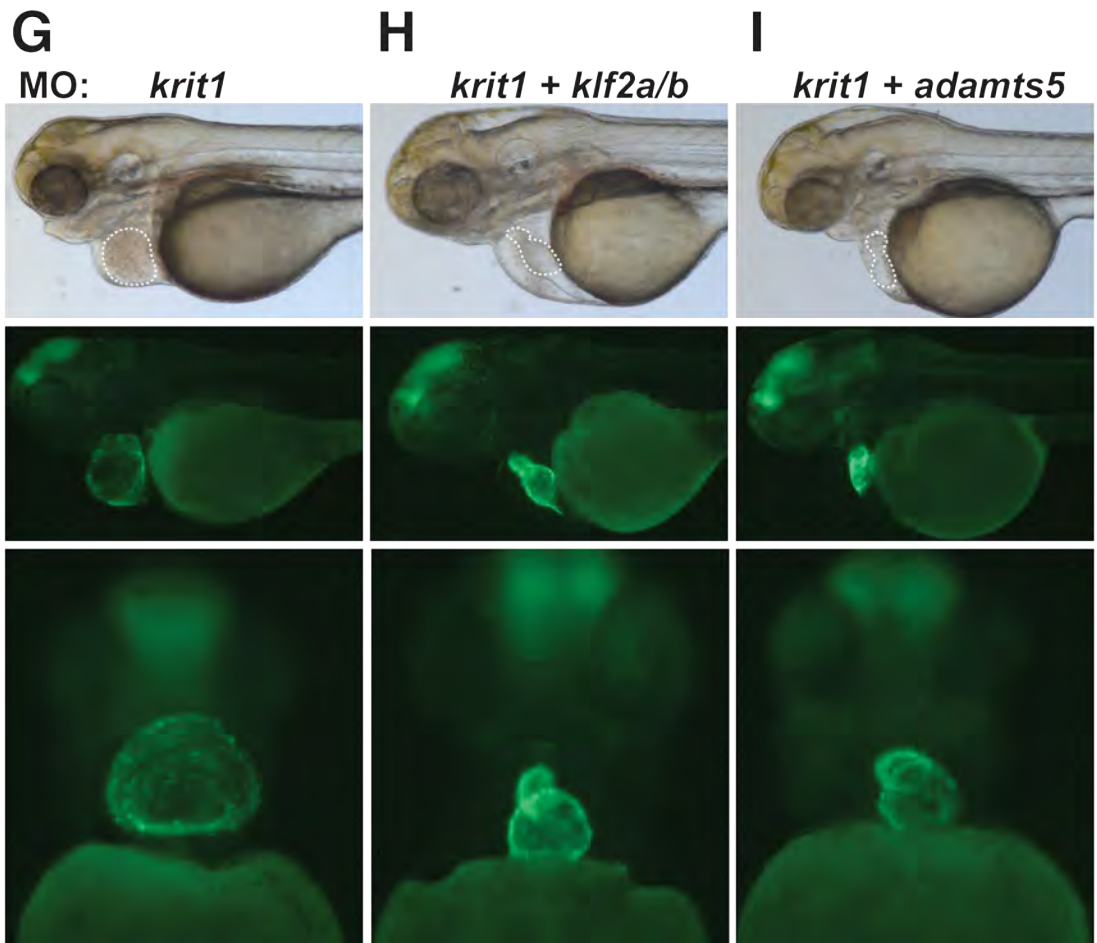
G
H
I
MO: krit1
krit1 + klf2a/b
krit1 + adamts5

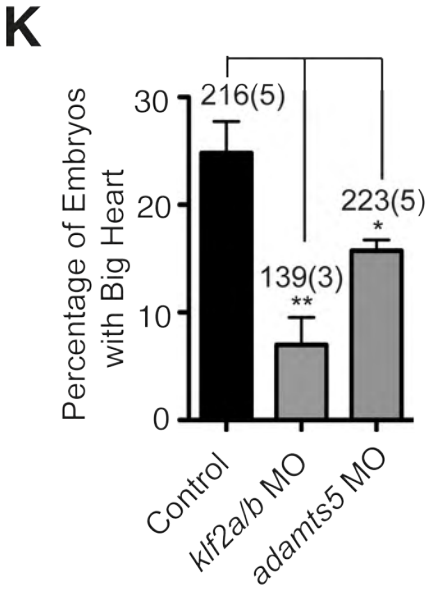
K
Percentage of Embryos with Big Heart
30
20
10
0
216(5)
139(3)
**
223(5)
*
Control
klf2a/b MO
adamts5 MO

Figure 5

Figure 5

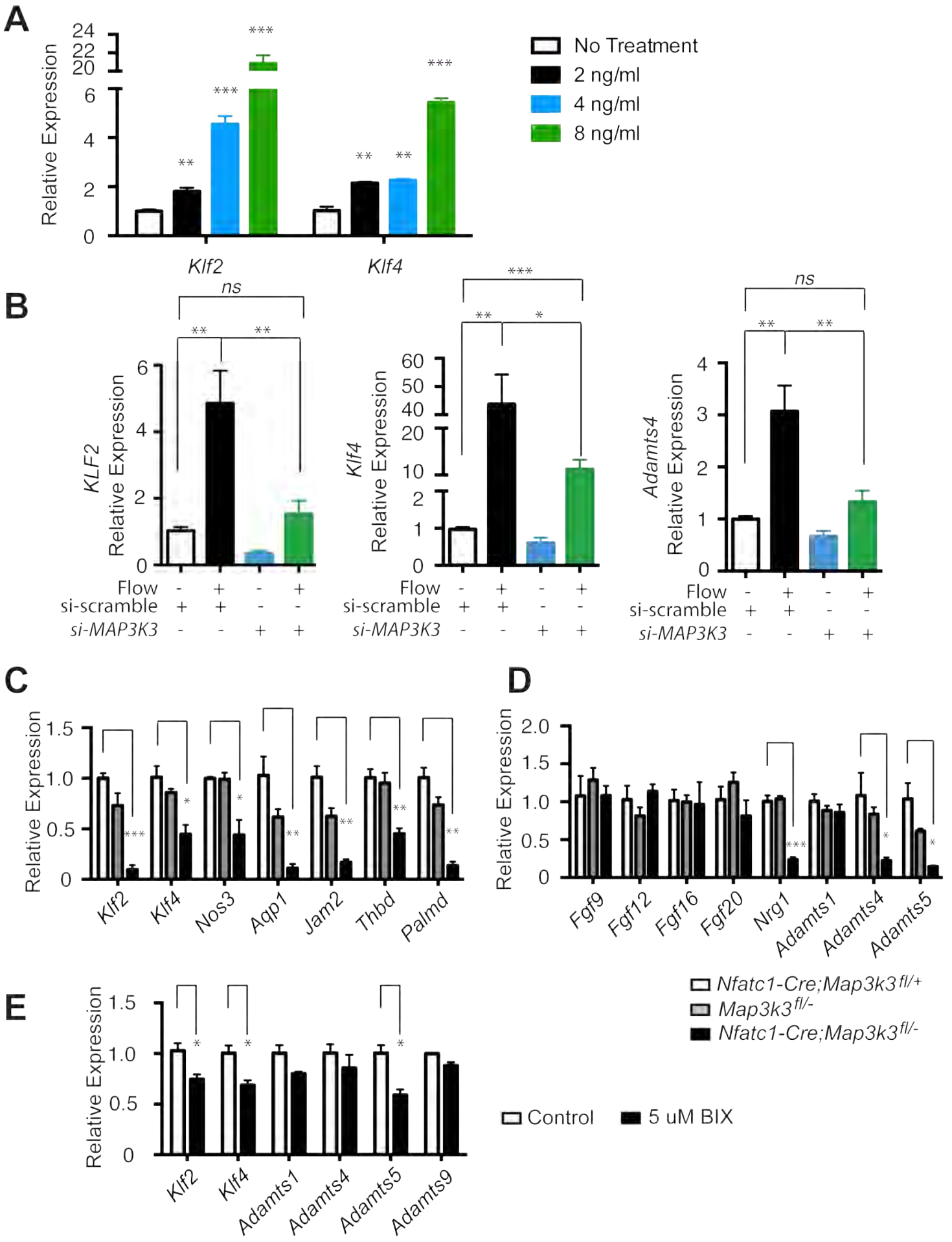

Figure 6

Figure 6

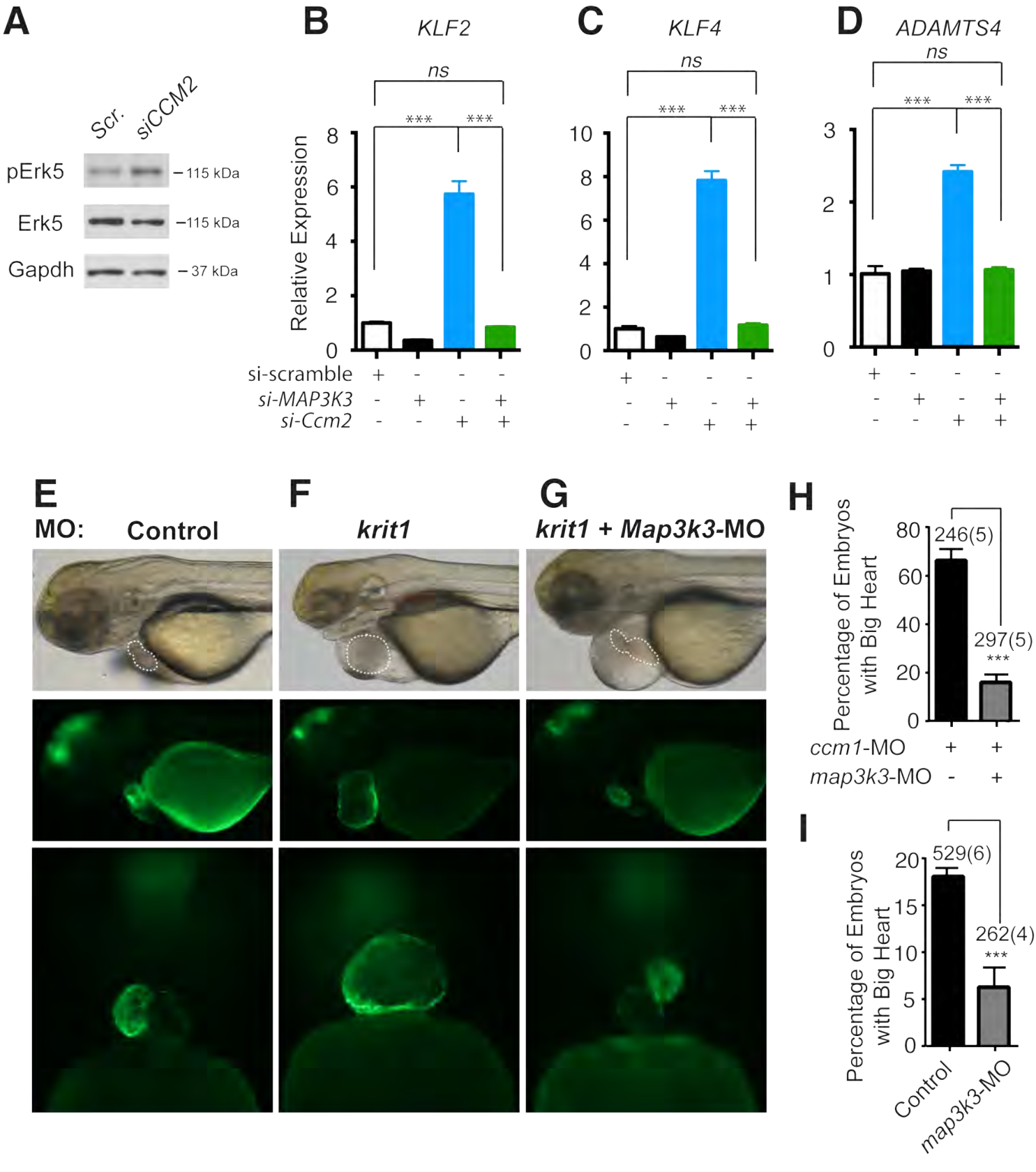

Figure 7

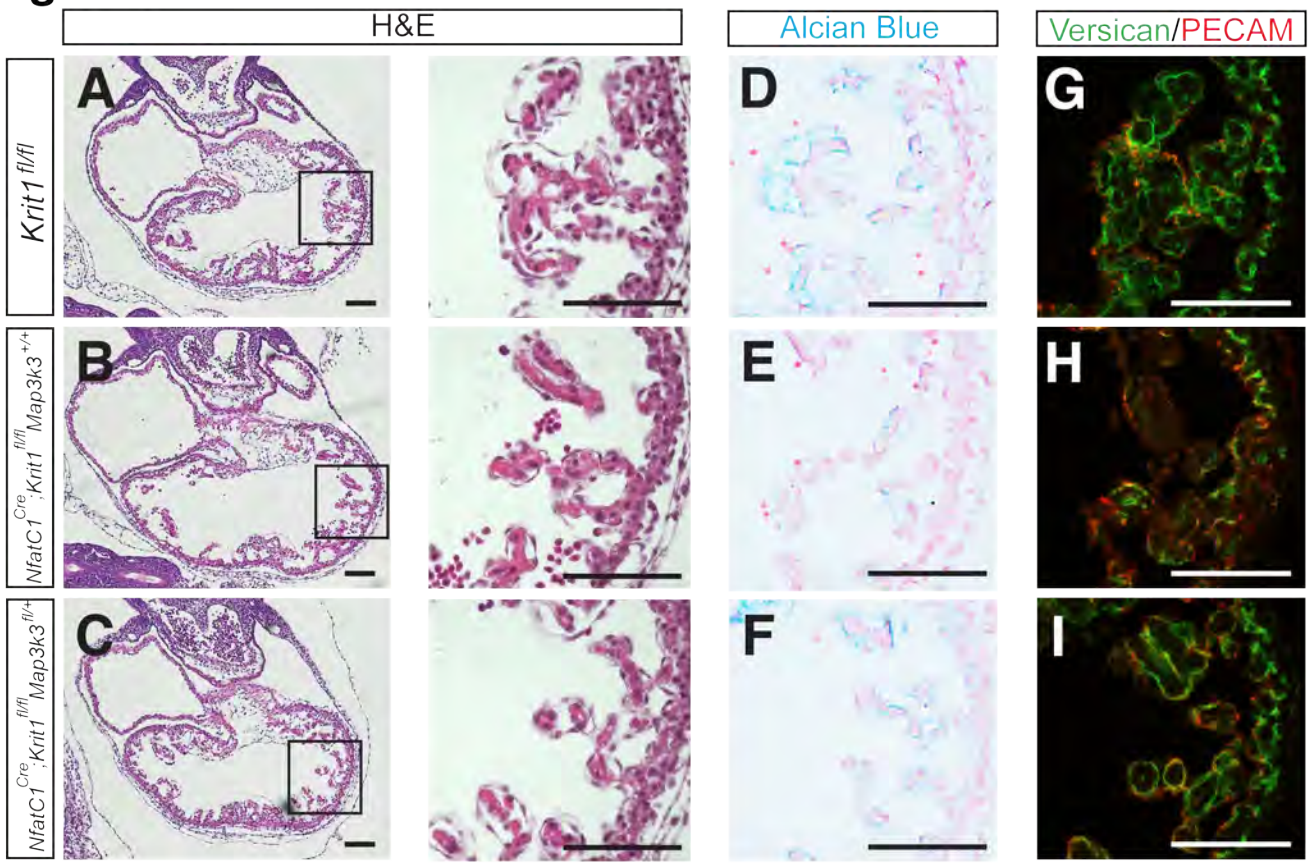
H&E
Alcian Blue
Versican/PECAM
Krit1 fl/fl
NfatC1 Cre ;Krit1 fl/fl Map3k3 +/+
NfatC1 Cre ;Krit1 fl/fl Map3k3 fl/+
A
B
C
D
E
F
G
H
I

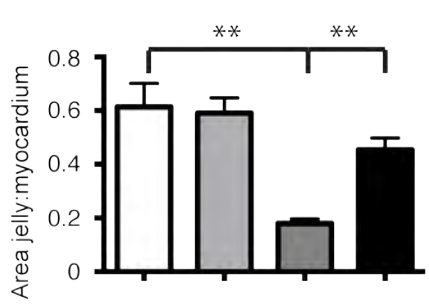
J
Area jelly:myocardium
0
0.2
0.4
0.6
0.8
**
**

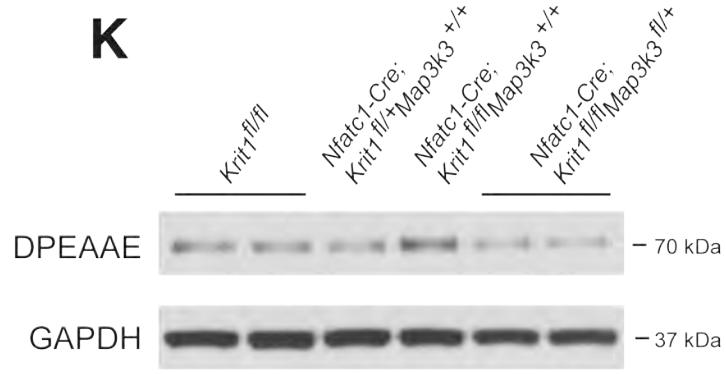
K
Krit1 fl/fl
Nfatc1-Cre; Krit1 fl/+Map3k3 +/+
Nfatc1-Cre; Krit1 fl/flMap3k3 +/+
Nfatc1-Cre; Krit1 fl/flMap3k3 fl/+
DPEAAE
70 kDa
GAPDH
37 kDa

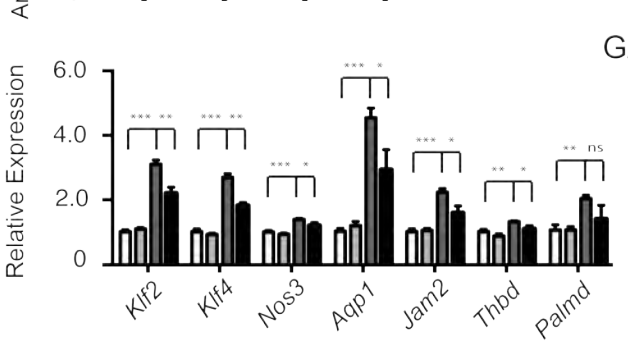
L
Relative Expression
0
2.0
4.0
6.0
Klf2
Klf4
Nos3
Aqp1
Jam2
Thbd
Palmd

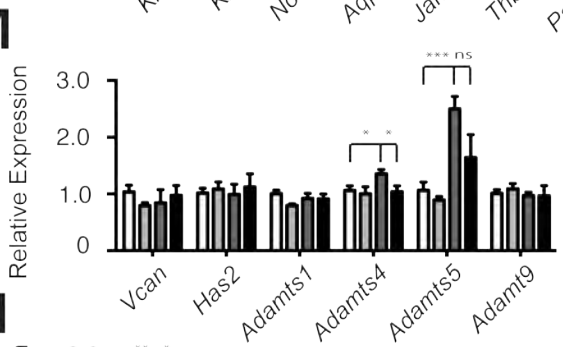
M
Relative Expression
0
1.0
2.0
3.0
Vcan
Has2
Adamts1
Adamts4
Adamts5
Adamtl9

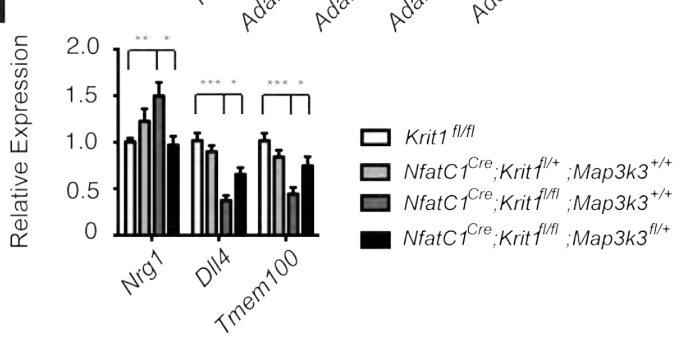
N
Relative Expression
0
0.5
1.0
1.5
2.0
Nrg1
Dll4
Tmem100
Krit1 fl/fl
NfatC1Cre;Krit1fl/+;Map3k3+/+
NfatC1Cre;Krit1fl/fl;Map3k3+/+
NfatC1Cre;Krit1fl/fl;Map3k3fl/+

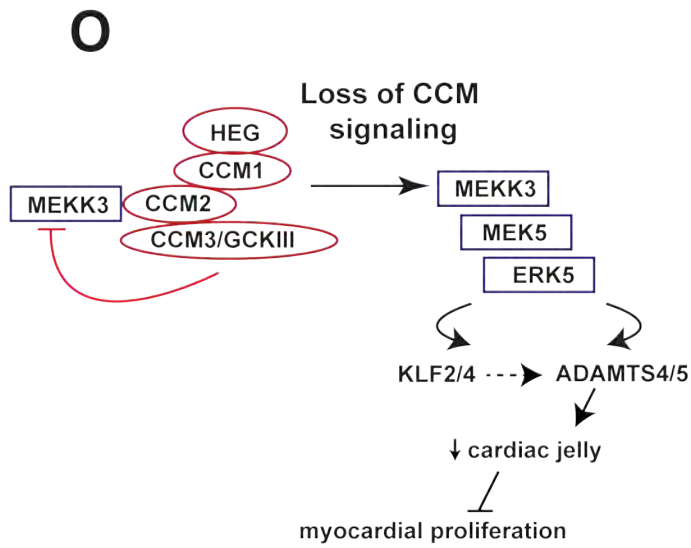
O
Loss of CCM signaling
HEG
CCM1
CCM2
CCM3/GCKIII
MEKK3
MEKK3
MEK5
ERK5
KLF2/4
ADAMTS4/5
cardiac jelly
myocardial proliferation

Supplemental Data

Figure S1

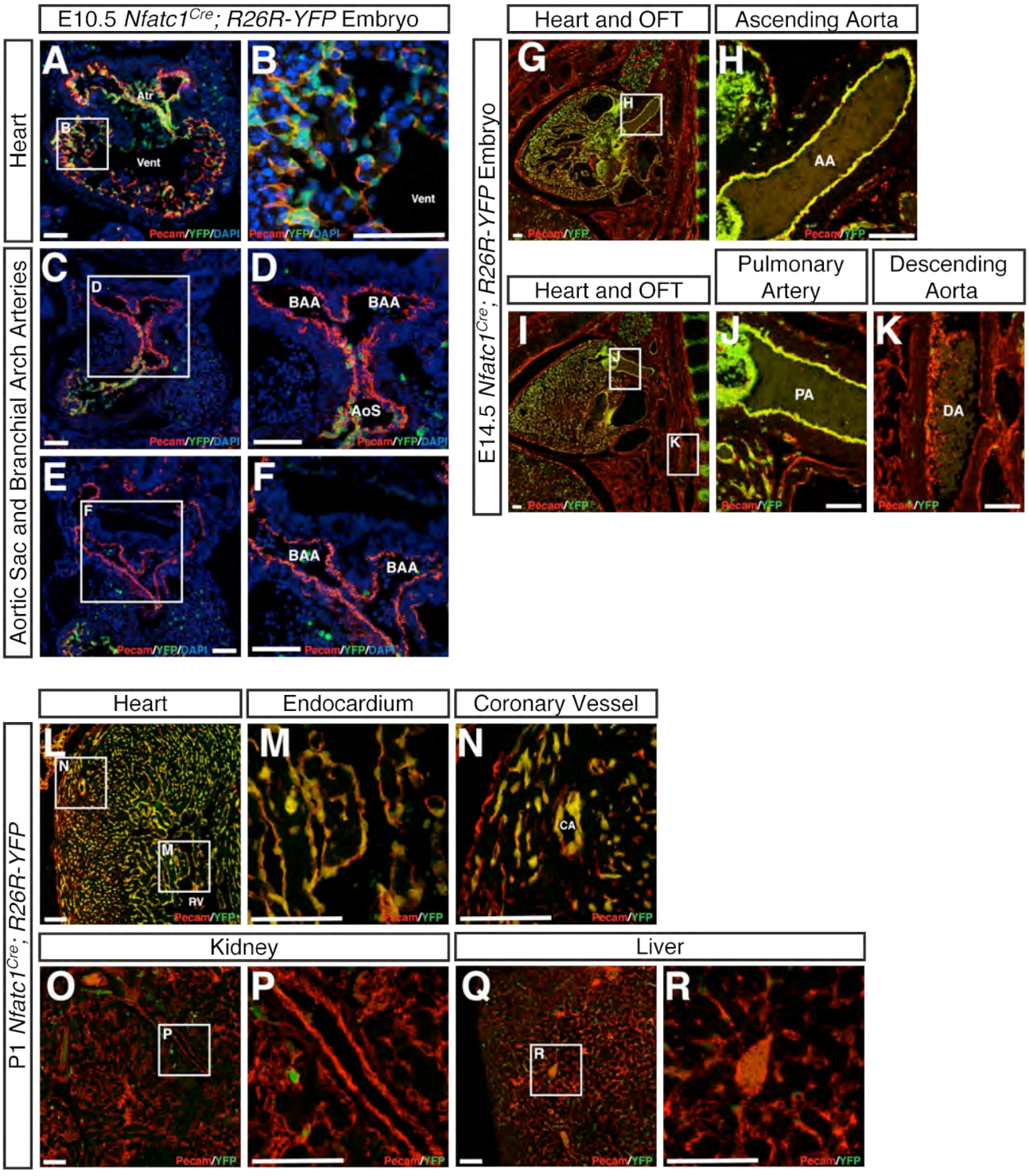

Figure S1. *Nfatc1*^{Cre} drives endothelial recombination in the heart but not in branchial arch arteries or peripheral vessels (related to Figure 1). A, B. Analysis of *Nfatc1*^{Cre}*;R26R-YFP* animals at E10.5 reveals uniform expression of YFP in the endocardium. **C-F.** *Nfatc1*^{Cre}

is not active in the endothelial cells that line the branchial arch arteries at E10.5. **G-K.** Analysis of *Nfatc1^{Cre};R26R-YFP* animals at E14.5 reveals endothelial YFP expression in the proximal aorta and pulmonary artery but not in the descending aorta. **L-R.** Analysis of *Nfatc1^{Cre};R26R-YFP* animals at P1 reveals YFP expression in endothelial cells of the cardiac chambers (L, M) and coronary arteries (N), but not the vasculature of the kidney (O, P) or liver (Q, R). BAA, branchial arch artery; AA, ascending aorta; PA, pulmonary artery; DA, descending aorta; CA, coronary artery. Scale bars indicate 100 μm.

Figure S2

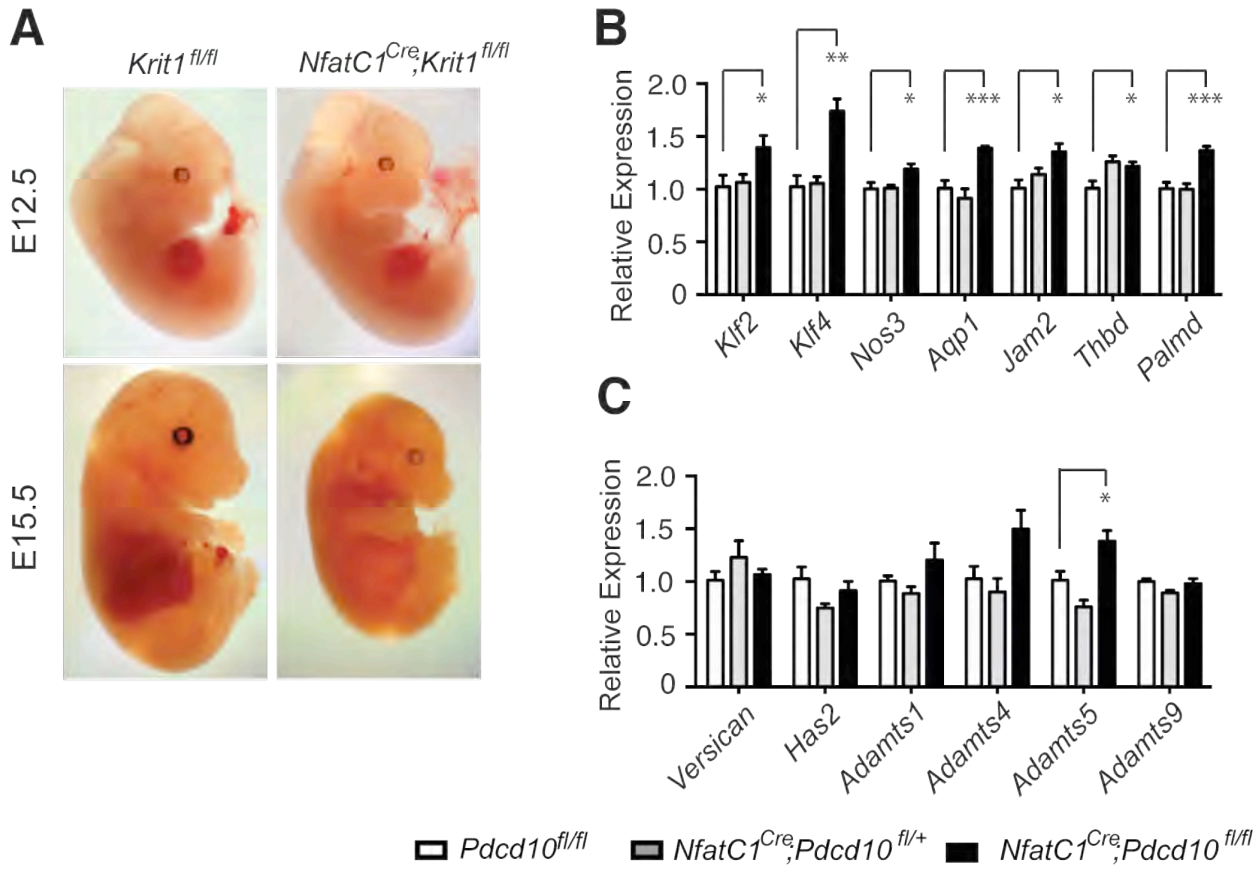

Figure S2. Survival of *Nfatc1^{Cre};Krit1$^{fl/fl}$* embryos and gene expression in *Nfatc1^{Cre};Pdcd10$^{fl/fl}$* embryos (related to Figures 1 and 2). **A.** *Nfatc1^{Cre};Krit1$^{fl/fl}$* embryos at E12.5 and 15.5. *Nfatc1^{Cre};Krit1$^{fl/fl}$* embryos were viable and visually indistinguishable from littermate controls at E12.5, but dead by E15.5. **B.** qPCR analysis of mRNA expression reveals increased levels of *Klf2*, *Klf4,* and KLF2/4 target genes in E10.5 *Nfatc1^{Cre};Pdcd10$^{fl/fl}$* compared with *Nfatc1^{Cre};Pdcd10$^{fl/+}$* and *Pdcd10$^{fl/+}$* littermate hearts like those seen with endocardial deletion of *Krit1*, but of lower magnitude. **C**. qPCR analysis of mRNA expression reveals increased levels of *Adamts4* and *Adamts5* with preserved levels of *versican* in E10.5 *Nfatc1^{Cre};Pdcd10$^{fl/fl}$* hearts as seen following endocardial deletion of *Krit1.* N= 4 for all genotypes. * indicates P <0.05; ** indicates P<0.01; *** indicates P<0.001; **** indicates P<0.0001.

Figure S3

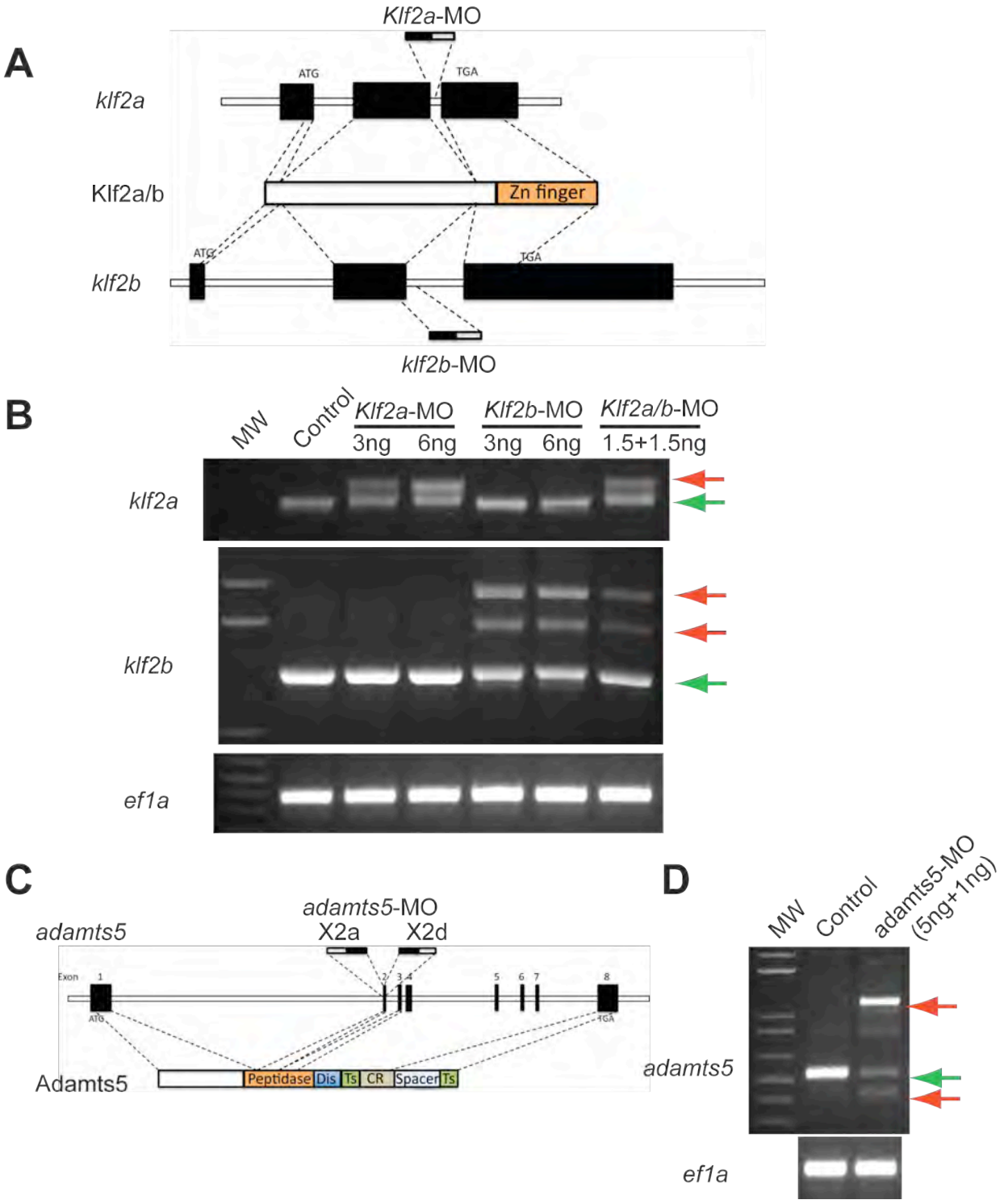

Figure S3. Characterization of *klf2* and *adamts5* morpholinos (related to Figure 4). A. Schematic diagram of morpholinos targeting the splice sites of the *klf2*a and *klf2*b genes in zebrafish. **B.** Characterization of knockdown efficiency of *klf2* morpholinos by RT-PCR of 30 hpf zebrafish embryos. In all cases the lower band, indicated by green arrows, is the amplified product of the wild-type mRNA while the upper bands, indicated by red arrows, are

those of mRNAs in which intron splicing has been blocked. The *ef1a* gene was amplified as a control. **C.** Schematic diagram of morpholinos targeting the splicing acceptor and donor sites of *adamts5* genes in zebrafish. **D.** Characterization of knockdown efficiency of *adamts5* morpholinos by RT-PCR of 30 hpf zebrafish embryos. The band indicated by green arrow is the amplified product of the wild-type mRNA while the upper band indicated by a red arrow is that of mRNAs in which intron splicing has been blocked, and the lower band indicated by a red arrow is the amplification of mRNA in which exon 2 splicing is skipped. The *ef1a* gene was amplified as a control.

Figure S4

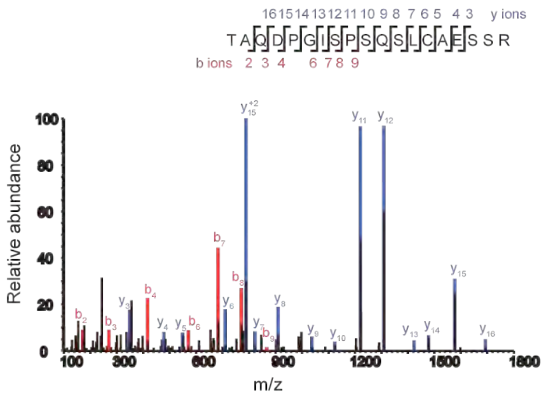

C

Start-End	Observed	Mr(expt)	Mr(calc)	ppm	Ion score	Sequence
147-154	465.7476	929.4807	929.4818	-1.18	42	R.DGEDIILR.V
147-154	465.7483	929.4821	929.4818	0.32	36	R.DGEDIILR.V
155-167	480.6053	1438.794	1438.7932	0.56	29	R.VPIHDIAAVSYVR.D
168-177	540.8058	1079.5971	1079.5975	-0.37	34	K.DDAAHLVVLK.T
168-177	540.8066	1079.5986	1079.5975	1.02	24	R.DDAAHLVVLK.T
178-196	995.9612	1989.9078	1989.9062	0.80	82	K.TAQDPGISPSQSLCAESSR.G
412-425	698.8365	1395.6585	1395.659	-0.36	39	R.ALSTTSSSTTNGNR.A
434-444	624.7609	1247.5073	1247.5054	1.52	36	R.SAPSEGDEWDR.M

D

```
1    MHSSCRQRRN QNLSKEIPQT EFHTGYSMEN EPGIVSPFKR VFLKGEKSRD
51   KKAHEKVTER RPLHTVVLSL PERVEPDRLL SDYIEKEVKY LGQLTSIPGY
101  LNPSSRTEIL HFIDNAKRAH QLPGHLTQEH DAVLSLSAYN VKLAWRDGED
151  IILRVPIHDI AAVSYVRDDA AHLVVLKTAQ DPGISPSQSL CAESSRGLSA
201  GSLSESAVGP VEACCLVILA AESKVAAEEL CCLLGQVFQV VYTESTIDFL
251  DRAIFDGAST PTHHLSLHSD DSSTKVDIKE TYEVEASTFC FPESVDVGGA
301  SPHSKTISES ELSASATELL QDYMLTLRTK LSSQEIQQFA ALLHEYRNGA
351  SIHEFCINLR QLYGDSRKFL LLGLRPFIPE KDSQHFENFL ETIGVKDGRG
401  IITDSFGRHR RALSTTSSST TNGNRATGSS DDRSAPSEGD EWDRMISDIS
451  SDIEALGCSM DQDSA
```

E

Protein	BirA peptide number	MEKK3-BirA peptide number
MEKK3	0	50
CCM2	0	11
SMTN	0	7
KRIT1	0	7
TRAF7	0	7

F

Protein	BirA peptide number	MEKK3-BirA peptide number
MEKK3	0	54
CCM2	0	11
KRIT1	0	21
TRAF7	0	11

Figure S4. MEKK3 interacts with CCM2 in endothelial cells (related to Figure 5). A. Immunodetection of tetracycline-induced expression of MEKK3-BirA and endogenous MEKK3 in hCMEC/D3 cells using anti-MEKK3 antibodies. **B.** MS/MS spectrum of an identified CCM2 peptide, TQDPGISPSQSLCAESSR. This peptide was doubly charged, and two fragment b and y ions (labeled by red and blue) were observed in the generated spectrum. **C.** Mass spectrometry identification result of CCM2. Six unique tryptic CCM2 peptides (total eight peptide-spectrum matches) were identified. “Start-End” refers to the position of the peptide in CCM2; “Observed” indicates the m/z (mass/charge) value detected by mass spectrometry; “Mr(expt)” indicates the detected molecular weight of the peptide; “Mr(calc)” indicates the theoretical molecular weight of the peptide; “ppm” represents the mass shift between “Mr(expt)” and “Mr(calc)”; “Ion score” is the Mascot score used to identify the peptide. **D.** Distribution of identified peptides in the CCM2 protein. Matched peptides are shown in red. The sequence coverage for CCM2 was 16%. **E, F.** Shown are the number of peptides of the indicated proteins detected by MS/MS analysis following streptavidin pulldown of hCMEC/D3 (E) or human umbilical vein (F) endothelial cells treated with 8 ng/ml doxycycline to induce expression of either BirA or BirA-MEKK3.

Figure S5

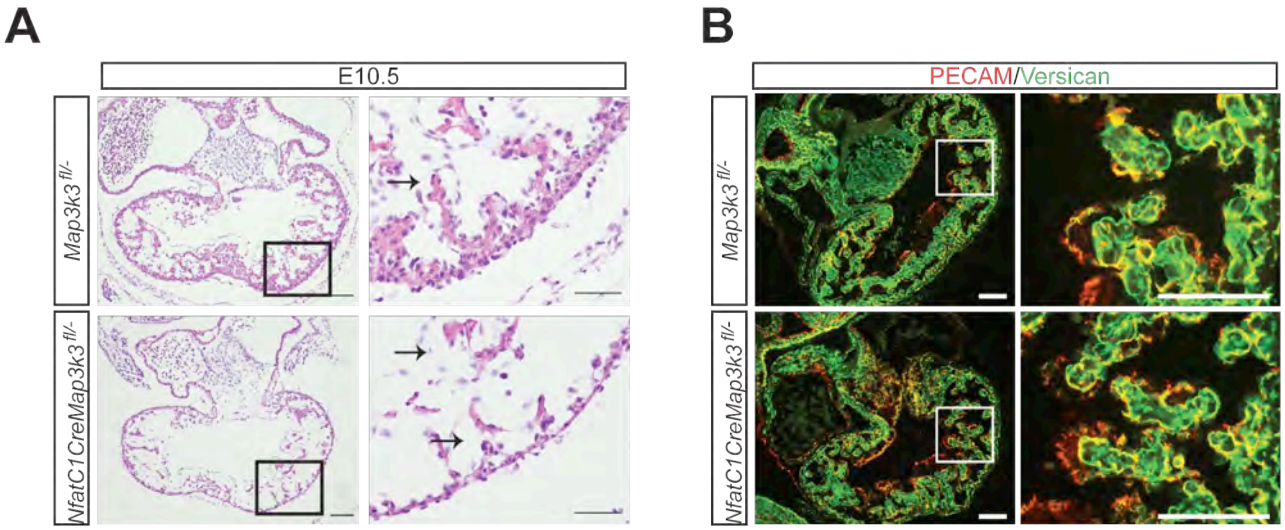

Figure S5. Endocardial loss of MEKK3 impairs cardiac development but does not alter cardiac jelly (related to Figure 5). A. *Nfatc1*^{Cre}*;Map3k3*$^{fl/-}$ hearts exhibit thinned myocardium and normal space between endocardial and myocardial cells at E10.5. Boxed regions are shown at higher magnification on the right. Arrows indicate the endocardial-myocardial gap. **B.** Immunostaining reveals preserved levels of versican in the E10.5 *Nfatc1*^{Cre}*;Map3k3*$^{fl/-}$ heart.

Figure S6

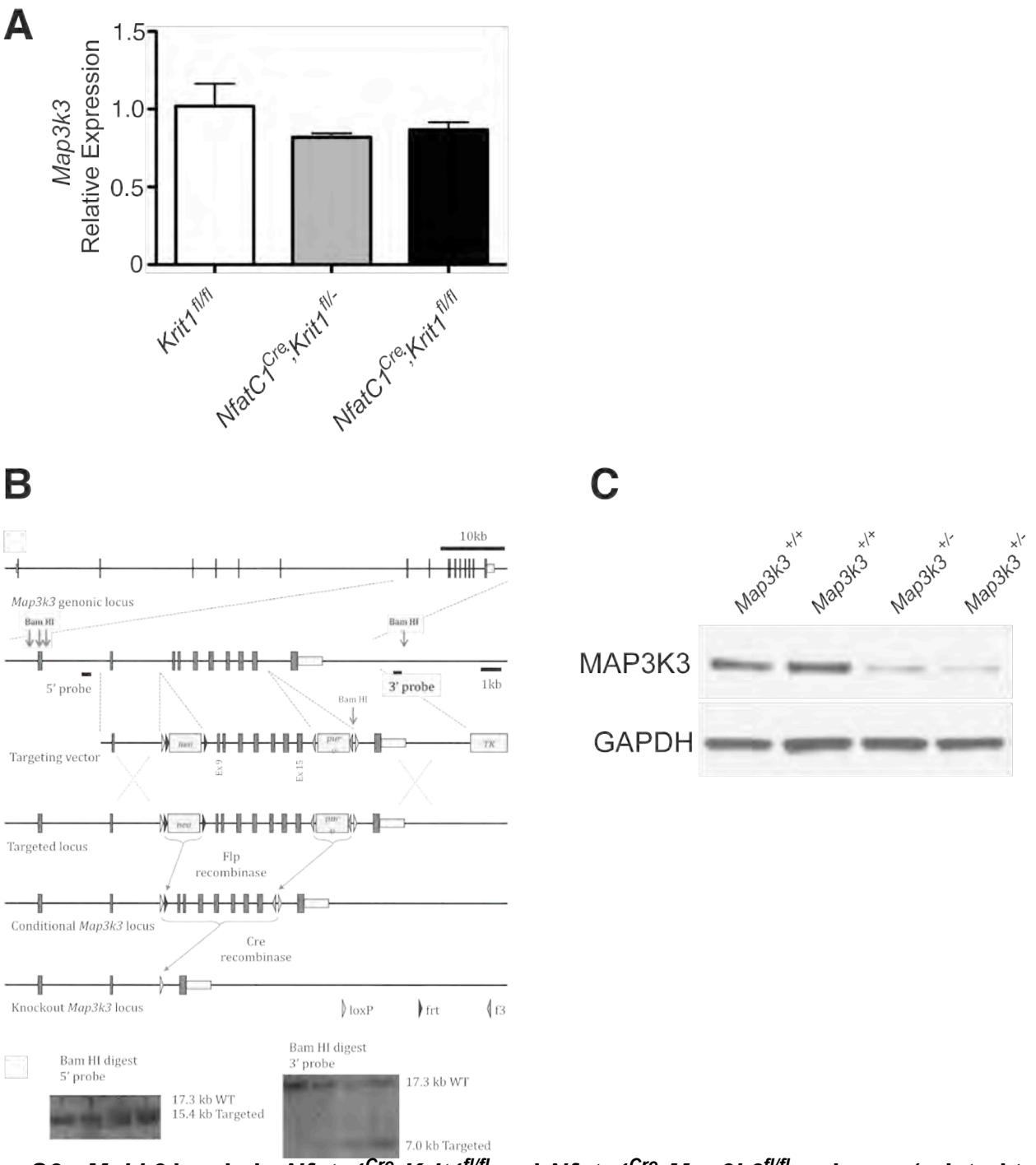

Figure S6. *Mekk3* levels in *Nfatc1*^{Cre}*;Krit1*$^{fl/fl}$ and *Nfatc1*^{Cre}*;Map3k3*$^{fl/fl}$ embryos (related to Figure 6). **A.** Hearts from *Nfatc1*^{Cre}*;Krit1*$^{fl/fl}$ and control embryos were harvested at E10.5 and qPCR performed to measure *Mekk3 (Map3k3)* mRNA levels. N=3; P>0.05. **B.** Generation of the *Map3k3*^{fl} allele. A targeting vector was constructed by recombinase mediated cloning to introduce loxP sites in introns 8 and 15. These were used to target Art B6.3.5 (C57BL/6 NTac) ES cells (top). Positive colonies were identified by Southern blotting and the presence of the point mutation confirmed by Southern bolts of genomic DNA digested with Bam HI using 5' and

3’ probes external to the targeting vector (bottom). **C.** MEKK3 protein levels are reduced in *Map3k3*$^{+/-}$ hearts. MEKK3 protein was detected using western blotting in E10.5 embryo hearts from littermates with the indicated genotypes. *Map3k3*$^{+/-}$ animals were generated by crossing *Map3k3*$^{+/fl}$ animals to EIIA-Cre transgenic animals to drive global gene deletion.

Figure S7

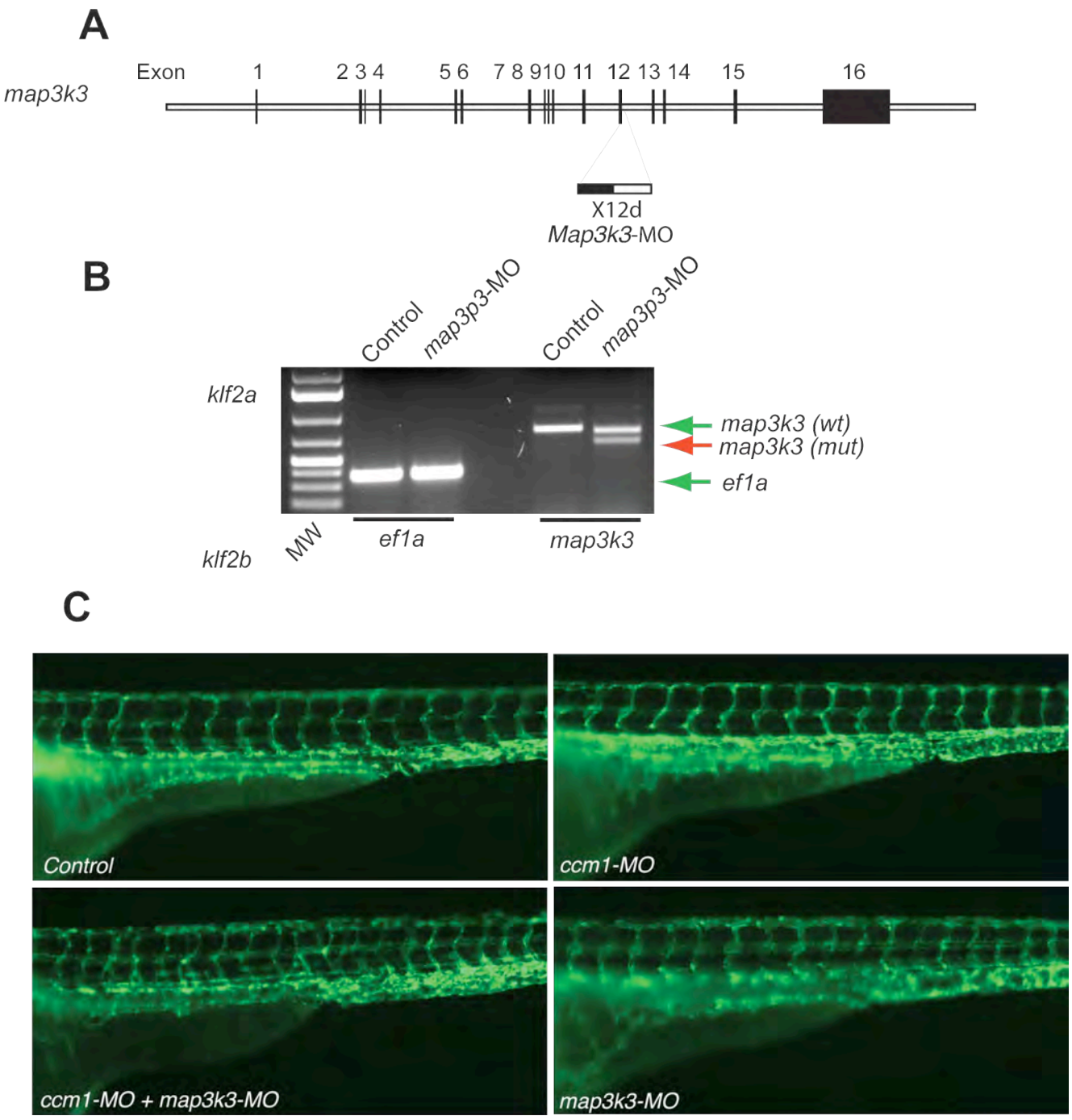

Figure S7. Characterization of *map3k3* morpholinos (related to Figure 7). A. Schematic diagram of the zebrafish *map3k3* allele and the exon 12 donor site targeted by *map3k3* morpholinos. **B.** Characterization of knockdown efficiency of *map3k3* morpholinos by RT-PCR of 30 hpf zebrafish embryos. The upper band, indicated by a green arrow, is the amplified product of the wild-type mRNA while the lower band, indicated by a red arrow, is that of

mRNAs in which intron splicing has been blocked. The *ef1a* gene was amplified as a control. **C.** Analysis of Fli1-GFP transgenic zebrafish reveals no disruption in vascular development in 72 hpf zebrafish embryos treated with low dose morpholinos targeting *krit1* and/or *map3k3*.

Table S1.

Live offspring of intercrosses between *Nfatc1^{Cre};Krit1/Ccm2/Pdcd10/Map3k3$^{fl/+}$* animals and *Krit1/Ccm2/Pdcd10/Map3k3$^{fl/fl}$* animals were genotyped at the indicated timepoints (related to Figures 1, 2 and 5).

	E10.5	**E12.5**	**E14.5**	**P0**
Total	60	18	24	37
Krit1$^{fl/+}$	21	5	9	14
Krit1$^{fl/fl}$	10	6	7	13
Nfatc1-Cre;Krit1$^{fl/+}$	13	3	8	10
Nfatc1-Cre;Krit1$^{fl/fl}$	**16**	**4**	**0***	**0****

	E10.5	**E12.5**	**P0**
Total	16	9	27
Ccm2$^{fl/+}$	4	1	6
Ccm2$^{fl/fl}$	5	2	13
Nfatc1-Cre;Ccm2$^{fl/+}$	3	3	8
Nfatc1-Cre;Ccm2$^{fl/fl}$	**4**	**3**	**0***

	E10.5-12.5	**E14.5**	**E15.5-17.5**	**P0**
Total	66	29	12	24
Pdcd10$^{fl/+}$	13	11	3	9
Pdcd10$^{fl/fl}$	19	9	6	9
Nfatc1-Cre; Pdcd10$^{fl/+}$	17	4	3	6
Nfatc1-Cre; Pdcd1$^{fl/fl}$	**19**	**5**	**0**	**0***

	E10.5	**E11.5**	**E14.5**	**P1**
Total	**100**	**55**	**51**	**54**
Map3k3fl/+	**29**	**15**	**16**	**14**
Map3k3fl/-	**29**	**23**	**11**	**19**
Nfatc1-Cre;Map3k3fl/+	**23**	**12**	**24**	**21**
Nfatc1-Cre;Map3k3fl/-	**19**	**5**	**0**	**0**

*** P<0.05; **P<0.001**

Supplemental Experimental Procedures

Gene expression analysis
Total RNA was isolated with RNeasy micro kit (Qiagen). Affymatrix mouse gene 2.0st chips were used for microarray analysis. For qPCR analysis, cDNA was synthesized from 1 μg total RNA using the Superscript III Reverse Transcriptase (Invitrogen). Real-time PCR was performed in Power SYBR Green PCR Master Mix (Applied Biosciences) using the primers listed below:

mKlf2 Forward - 5'- CGCCTCGGGTTCATTTC -3'
mKlf2 Reverse - 5'- AGCCTATCTTGCCGTCCTTT -3'
mKlf4 Forward - 5'- GTGCCCCGACTAACCGTTG-3'
mKlf4 Reverse - 5'- GTCGTTGAACTCCTCGGTCT-3'
mAqp1 Forward - 5'- CATCACCTCCTCCCTAGTCG -3'
mAqp1 Reverse - 5'- CAGTACCAGCTGCAGAGTGC -3'
mJam2 Forward - 5'- GATCGTCGCCCTGGACTATC -3'
mJam2 Reverse - 5'- GTGACTTCTTGACGGTGGTCT -3'
mThbd Forward - 5'- CTCTCCGCACTAGCCAAGC -3'
mThbd Reverse - 5'- GGAGCGCACTGTCATCAAATG -3'
mPalmd Forward - 5'- ATCTCACAGAAGCGTCTGAAAAT -3'
mPalmd Reverse - 5'- CTGCCGATTCCATCCAGGAG -3'
mNrg1 Forward - 5'- GAAGAAGCCAGGGAAGTCAGAGCT -3'
mNrg1 Reverse - 5'- TGGCTGGTCCCAGTCGTGGATGT -3'
mFgf9 Forward - 5'- GCTCATTGTGGAGACCGATACTT -3'
mFgf9 Reverse - 5'- TGGCAATTAGCTTCCCCTTCT -3'
mFgf12 Forward - 5'- ACAGCGACTACACCCTCTTCA -3'
mFgf12 Reverse - 5'- CTGTTCCCCTTCATGATTTGA -3'
mFgf16 Forward - 5'- GCTTCCACCTTGAGATCTTCC -3'
mFgf16 Reverse - 5'- ACTGTTCCCGGAAAACACATT -3'
mJag1 Forward - 5'- TGGCCGAGGTCCTACACTT -3'
mJag1 Reverse - 5'- GCCTTTTCAATTATGCTATCAGG -3'
mDll4 Forward - 5'- AGGTGCCACTTCGGTTACAC -3'
mDll4 Reverse - 5'- GGGAGAGCAAATGGCTGATA -3'
mTmem100 Forward - 5'- GACAATGGAGAAAAACCCCAAGA -3'
mTmem100 Reverse - 5'- GGTAGCAGGAGAGTTCGGC -3'
mVersican Forward - 5'- ACTAACCCATGCACTACATCAAG -3'
mVersican Reverse - 5'- ACTTTTCCAGACAGAGAGCCTT -3'
mHas2 Forward - 5'- TGGGGTGGAAAGAGAGAAGT -3'
mHas2 Reverse - 5'- ACAGATGAGGCAGGGTCAAG -3'
mAdamts1 Forward - 5'- CTCTCACCCTTCGGAATTTCTG -3'
mAdamts1 Reverse - 5'- GGAGCCACATAAATCCTGTCTG -3'
mAdamts4 Forward - 5'- CAGTGCCCGATTCATCACT -3'
mAdamts4 Reverse - 5'- GAGTCAGGACCGAAGGTCAG -3'
mAdamts5 Forward - 5'- CGACCCTCAAGAACTTTTGC -3'
mAdamts5 Reverse - 5'- CGTCATGAGAAAGGCCAAGT -3'
mAdamts9 Forward - 5'- TTGGGACCTGCTCAAGAACG -3'
mAdamts9 Reverse - 5'- ACCATTGATGTTGAAGTGTTTGC -3'

Biotinylation of BirA-MEKK3 interacting proteins in live endothelial cells.

MEKK3 was PCR-amplified from pCMV5-MEKK3 (Addgene plasmid 12186). HA-BirA was PCR-amplified from mycBioID (Addgene plasmid 35700). The two fragments were ligated to create HA-BirA-Mekk3 and cloned into the NotI and MluI sites in the pLVX-TRE3G vector (Invitrogen). For a control, BirA-HA was PCR-amplified from MCS-BirA(R118G)-HA (Addgene plasmid 36047), and cloned into the ApaI and NotI sites in the pLVX-TRE3G vector. hCMEC/D3, an immortalized human brain microvessel endothelial cell line, was grown as previously described (Weksler et al., 2005), cotransduced with both the LVX-TRE3G and LVX-Tet3G lentiviruses, and selected by G418 and puromycin. Stably transduced hCMEC/D3 cells were cultured in doxycycline-containing medium (8 ng/ml) for 3 days to express BirA-Mekk3, biotinylation induced as previously described (Roux et al., 2012), and biotinylated proteins immunoprecipitated.

Identification of BirA-MEKK3 interacting proteins using NanoLC-MS/MS analysis
The beads were resuspended in 30ul urea solution (8M urea, 75mM NaCl and 50mM Tris-HCl, pH8.3). DTT (10mM) and iodoacetamide (40mM) were added sequentially to reduce and alkylate cysteine on proteins. The solution was diluted to 1.5M urea using 50mM Tris-HCl (pH8.3). Trypsin (Promage) was added at a ratio of 1:50 (w/w) and proteins were digested overnight at room temperature. The beads were kept rotated on a rotator during all above steps. After digestion, peptides were desalted using Sep-Pak C18 cartridges (Waters) and the eluates were lyophilized.
NanoLC-MS/MS analysis: NanoLC-MS/MS was performed on a Q Exactive (Thermo Scientific) mass spectrometer equipped with EASY-nLC 1000 HPLC. Lyophilized samples were dissolved in Buffer A (0.1% formic acid in water) and loaded to a homemade C18 analytical column (75 μm I.D. × 200 mm) packed with ReproSil-Pur C18-AQ 3 μm resin (Dr. Maisch GmbH). A 120min LC gradient from 5 to 35% Buffer B (0.1% formic acid in acetonitrile) was used to separate peptides at a flow rate of 300 nL/min. The full MS scan range was m/z 350–1600. The top 15 precursor ions were selected to perform MS/MS scans by high-energy collisional dissociation (HCD). Automated gain control (AGC) values were 1E6 and 1E5 for full MS and MS/MS scans, respectively. Normalized HCD energy was set to 22.0. Dynamic exclusion was enabled with the exclusion time of 30 sec. Lock mass calibration in full MS scan was implemented using polysiloxane ion, 371.10123.
Data analysis: The acquired MS/MS spectra were searched through Mascot engine against the human Uniprot database consisting of forward and reversed protein sequences. The precursor ion tolerance was set to 10 ppm, and the fragment ion tolerance was set to 0.02 Da. Carbamidomethylation (57.0215) of cysteine was considered as a static modification, and biotinylation (226.0776) of lysine, oxidation (226.0776) of methionine and acetylation (42.0106) of protein N-terminus were considered as dynamic modifications. 1.0% False Discover Ratio (FDR) was used to filter the identified peptides.

Morpholino sequences
ccm1-MO: 5’- TGACCACCACTAACCTATTATGCCC-3’

klf2a-MO: 5’- AACAAGTGGCGTTTATTTACCTGTG-3’

klf2b-MO: 5’- TAAAATGCATTCTTACCGGTGTGAG-3’

adamts5-MO (X2a): 5’- CCCGCACAGATCCTGAATACACACA-3’

adamts5-MO (X2d): 5’-GTCTATGATCCGTCTGTGTACCGAT-3’

map3k3-MO 5'-AAACATGTACCTTGCTGGTCTCTGG-3'

Primers used for qPCR analysis of cultured human endothelial gene expression
MAP3K3 Forward: 5'-AGGCATTAGACTCGATCATGAAG-3'
MAP3K3 Reverse: 5'-CTCCCCATTGTGTTCAAACTTG-3'
KLF2 Forward: 5'-CTACACCAAGAGTTCGCATCTG-3'
KLF2 Reverse: 5'-CCGTGTGCTTTCGGTAGTG-3'
KLF4 Forward - 5'- AGAGTTCCCATCTCAAGGCA -3'
KLF4 Reverse - 5'- GTCAGTTCATCTGAGCGGG -3'
ADAMTS4 Forward - 5'- CTGACTTCCTGGACAATGGC -3'
ADAMTS4 Reverse - 5'- GCGGTCAGCATCATAGTCCT -3'

References for Supplemental Experimental Procedures

Roux, K.J., Kim, D.I., Raida, M., and Burke, B. (2012). A promiscuous biotin ligase fusion protein identifies proximal and interacting proteins in mammalian cells. J Cell Biol *196*, 801-810.

Weksler, B.B., Subileau, E.A., Perriere, N., Charneau, P., Holloway, K., Leveque, M., Tricoire-Leignel, H., Nicotra, A., Bourdoulous, S., Turowski, P.*, et al.* (2005). Blood-brain barrier-specific properties of a human adult brain endothelial cell line. Faseb J *19*, 1872-1874.